IOP Publishing Biofabrication 18 (2026) 015031 https://doi.org/10.1088/1758-5090/ae3d85

Biofabrication

OPEN ACCESS

RECEIVED
30 August 2025

REVISED
3 November 2025

ACCEPTED FOR PUBLICATION
26 January 2026

PUBLISHED
5 February 2026

PAPER

A mechanically active nucleus pulposus-on-a-chip for studying mechanobiology and therapeutic strategies in intervertebral disc disease

Olga Krupkova[1,2], Bianca Aterini[1,3], Nader Rahal[3], Elias Schulze[4], Salim Darwiche[5], Martin Ehrbar[6,7], Karoliina Pelttari[1], Ivan Martin[1], Stefan Schären[2], Arne Mehrkens[1,2,*], Andrea Barbero[1] and Andrea Mainardi[1,*]

[1] Department of Biomedicine, University Hospital Basel, University of Basel, Hebelstrasse 20, 4031 Basel, Switzerland
[2] Spine Surgery, University Hospital Basel, Spitalstrasse 21, 4031 Basel, Switzerland
[3] Department of Electronics, Information and Bioengineering, Politecnico di Milano, Via Golgi 39, 20133 Milan, Italy
[4] Institut für Pathologie, University Hospital Basel, Schönbeinstrasse 40, 4031 Basel, Switzerland
[5] Musculoskeletal Research Unit (MSRU), University of Zurich, Winterthurerstrasse 190, 8057 Zürich, Switzerland
[6] Department of Obstetrics, University Hospital Zürich, Frauenklinikstrasse 10, 8091, Zürich, Switzerland
[7] Zürich Centre for Integrative Human Physiology, Winterthurerstrasse 190, 8057 Zürich, Switzerland
[*] Authors to whom any correspondence should be addressed.

E-mail: arne.mehrkens@usb.ch and andrea.mainardi@dpag.ox.ac.uk

Keywords: intervertebral disc degeneration, nucleus pulposus, mechanobiology, mechanotransduction, organ-on-chip

Abstract

Intervertebral disc (IVD) degeneration is the primary contributor to low back pain, the leading cause of disability worldwide. Although various triggers have been associated with IVD degeneration, its precise aetiology remains unclear. Consequently, current treatments fail to address the underlying degradative processes. Mechanical loading plays a critical role in IVD homeostasis, and aberrant mechanical stimulation has been identified as a key driver of extracellular matrix degradation in the proteoglycan-rich core of the IVD—the nucleus pulposus (NPs). Elucidating the molecular mechanisms of IVD mechanotransduction could therefore be pivotal in identifying effective drug targets. However, we are lacking easy-to-use, reliable models to study IVD's mechanobiological mechanisms in human cells. Here, we present the first mechanically active, microscale, human cell-based NP-on-a-Chip (NPoC) model that mimics the native NP microenvironment and enables controlled investigation of mechanically induced degenerative processes. Starting from primary human NP cells, we demonstrate that hypoxic culture (i.e. 2% O_2) results in 3D constructs with gene expression levels of NP markers (*ACAN, COL2A1, CDH2, OVOS2*), and matrix composition (collagen type II and glycosaminoglycans) comparable with the native NP tissue. NPoC constructs respond to cyclic compression in an intensity- and duration-dependent manner. Physiological compression (10%) enhances glycosaminoglycan deposition, whereas hyperphysiological compression (30%), especially if prolonged in time (16 h d^{-1}), induces upregulation of inflammatory and catabolic markers (*PTGS2, MMP13*), matrix degradation, and increased apoptosis—thus recapitulating clinical hallmarks of NP degeneration. As a proof of concept for the platform's perspective utility in therapeutic screening, we demonstrate that inhibition of the mechanoresponsive channel TRPV4 with GSK205 restores baseline expression levels of mechanosensitive and catabolic genes. The new NPoC is thus suitable for studying NP mechanobiology and screening mechanotransduction-targeting drugs, and it may facilitate the future discovery of disease modifying therapies for discogenic low back pain.

1. Introduction

Low back pain (LBP) is a global cause of disability with a lifetime prevalence of 84% and 23% of individuals developing chronic symptoms [1]. Direct and indirect LBP costs in high-income countries are estimated, respectively, at €2.6 billion and $8.15 billion [2].

The most common cause of LBP is intervertebral disc (IVD) degeneration (IDD), accounting for 40% of registered cases [3]. IDD pathological changes include a decrease in water and glycosaminoglycans (GAGs) content in the nucleus pulposus (NPs), augmented levels of cytokines and chemokines (e.g. IL-1β, TNF-α, IL-6, IL-8), secretion of nociceptive factors [4], an anabolic/catabolic imbalance (marked by a decrease in type II collagen and aggrecan, and an increased in matrix-degrading metalloproteinases (MMPs) and aggrecanases), ectopic ingrowth of nerves and blood vessels, immune cells infiltration [4], and cellular senescence and apoptosis [5].

While IDD's progression has been well described, its precise aetiology remains unknown. Age, gender, previous injuries, and genetics have all been listed as IDD contributors [5, 6]. Yet, multiple lines of evidence point to a strong association between IDD and mechanical risk factors, such as excessive axial loads, obesity, spinal misalignment, and occupational hazards (e.g. prolonged vibration from riding in or operating motorised vehicles and machinery [7–9]). This highlights the need for further research into the mechanisms and effects of mechanical loading in IVD pathophysiology.

IVDs are continually mechanically stimulated during daily activities via spinal flexion, extension, torsion, and muscle activation. IVDs' functional anatomy itself evolved to resist mechanical loading. The outer annulus fibrosus (AF), composed of concentric lamellae of type I collagen fibres, resists tension during flexion and torsion. The inner NP, composed of highly hydrated proteoglycans (PGs) and collagen type II [10], responds to compression through osmotic and pressure changes [7, 11, 12]. In general, physiological mechanical loading enhances nutrient exchange and matrix homeostasis [12–14], whereas both mechanical overload and immobilisation [15] cause molecular, cellular, and structural damage [12, 14], NP cells apoptosis [16], and secretion of inflammatory and nociceptive factors [17]. In general, IVD's responses to mechanical stimuli depends on the strain magnitude, coexisting stresses, and loading frequency and pattern [10].

Pioneering mechanotransduction molecular studies established a correlation between IDD and signalling by the transcriptional coactivators MRTF-A and YAP/TAZ [18, 19]; as well as between transient receptor potential channels [20–22], disc degeneration [21], and transduction of inflammatory pain [20]. However, despite the unprecedented insights into IVD biology provided by omics analyses [6, 23], the mediators involved in aberrant mechanosensing and mechanotransduction within the IVD remain poorly understood [13]. This knowledge gap is, at least partially, due to the absence of satisfactory preclinical models to dissect these phenomena in human IVDs.

Animal models can replicate the disease complexity but, with distinctions between small and large species [24], they may differ in size, genetic background, biomechanics, and cell composition with respect to human counterparts [23, 25]. Moreover, ethical considerations (i.e. the 3Rs principles) urge the use of alternative models. Conversely, classic *in vitro* 2D cultures, although more controllable, often fail to reproduce physiological conditions [14].

Recently developed macroscale bioreactors better mimic the *in vivo* environment by applying tension, compression, shear, or combinations thereof to either *ex vivo* whole-organ IVDs ([26]) or biomaterial-based engineered tissues [27]. Yet, these models require bulky instrumentations and whole animal or human IVDs, which suffer from availability issues, limiting their use for comprehensive mechanistic studies and large drug screenings. Significant challenges remain, therefore, in developing suitable preclinical models to elucidate mechanotransduction pathways and predict therapeutic efficacy in loaded human IVDs [12].

Organ-on-Chip models (OoCs) are microscale devices aiming at replicating organ and tissue level functions *in vitro* [28, 29]. Leveraging on soft lithographic methods [30], OoCs can mimic multicellular architectures, tissue–tissue interfaces, and physicochemical microenvironments [31–34], reaching levels of tissue and organ functionality unattainable with conventional systems [29]. In the context of IVD studies, the microscale nature of OoC devices (which operate with nano- to microliter fluid volumes and require minimal cells and reagents) would allow to scale up the number of experiments that can be conducted and of scientific questions that can be addressed.

Nonetheless, as we [10] and others [35, 36] previously reviewed, only a few attempts were made at developing OoC IVD models. Pioneering IVD-on-a-Chip studies examined phenomena ranging from AF cells' inflammatory reactions [37] to the interactions between NP cells and nociceptor-like sensory neurons [4], but were based on non-physiological 2D geometries. Early attempts to integrate IVDs' 3D architecture and mechanical stimuli involved applying shear stress to whole-organ IVDs from small animals (mouse/rabbit) [38, 39]. Other studies explored how flow rate and electrical stimulation influence IVD cells using multichannel devices [40, 41]. While these efforts demonstrated that microfluidics can support IVD research, the majority of existing models suffer from drawbacks such as being based on 2D cell

monolayers, inadequate representation of the IVD extracellular matrix (ECM) microenvironment [37], or the use of species with low translational relevance [10, 38]. A recent work introduced a more advanced human-based microscale IVD-model, permitting to study the interactions between different cell types in a 3D environment [42]. However, to the best of our knowledge, no existing OoC IVD model incorporates physiologically relevant mechanical stimulation.

To address these shortcomings, we aimed to develop an easy-to-use, mechanically active OoC platform, where microscale 3D cellular constructs based on human cells can be exposed to physiological (i.e. 10%, in the range of diurnal disc height variations in healthy subjects [43]) or hyperphysiological (i.e. 30%) cyclic compression, to investigate the effect of mechanical stimuli on IVD physiopathology and, prospectively, screen promising IDD drug candidates.

Specifically, as a first step towards a complete IVD-on-Chip, we aimed to establish a reductionist NP-on-a-Chip (NPoC) model, to determine if physio-pathological mechanical compression could elicit initial IDD-like changes observed in the NP, such as loss of PGs, matrix degradation, and decreased cellularity.

Leveraging on the gas permeability of the device, we investigated the oxygen levels required to obtain 3D constructs with native-like gene expression and ECM composition. We then assessed the effects of different compression levels and stimulation regimens on the expression of mechanotransduction marker genes and on the acquisition of an IDD–like phenotype in NP-like constructs. Finally, we evaluated the therapeutic potential of inhibiting mechanotransduction signalling mediated by the transient receptor potential cation channel subfamily V member 4 (TRPV4), providing a proof of concept for the capabilities of the NPoC to be used as an effective drug screening tool.

2. Results

2.1. Device concept

The highly hydrated and glycosaminoglycans-rich environment of the NP makes it an ideal structure to withstand compressive loading [44]. Excessive compression levels were however demonstrated to alter NP cells' physiology [45].

Leveraging a proprietary mechanical actuation technology [34], we developed a strain-controlled NPoC model capable of providing 3D constructs based on human NP cells with either physiological compression (PC, i.e. 10%) or hyperphysiological compression (HPC, i.e. 30%).

The microscale platform features three identical culture chambers, so that a triplicate of independently cultured constructs can be obtained with a single device (figure 1(A)). Each chamber is composed of three layers: a cell culture compartment, an actuation membrane, and an actuation chamber (figures 1(A) and (B)). The cell culture compartment comprises a central channel hosting a cell-laden hydrogel, and two lateral culture medium channels connected to medium reservoirs. The three channels are divided by two rows of T-shaped overhanging pillars. The height of the pillars is lower than the overall height of the chamber (10% version: pillar height = 129 μm, chamber height 143 μm; 30% version: pillar height = 100 μm, chamber height 143 μm). Upon application of a positive pressure in the actuation chamber, the actuation membrane deflects upward, until it is stopped by the bottom surface of the pillars (figure 1(C)). The final displacement of the membrane, and consequently the compressive strain of the construct hosted in the central channel, depend therefore only on the difference in height between the pillars and the whole chamber, making our device strain -controlled, as previously demonstrated by our group [34, 46]. Adopting devices with different internal heights (namely the 10% and the 30% versions, figure 1(C)), platforms that provide finely controlled compression levels are obtained. Of note, in this manuscript we use 'strain' as a general term for deformation, so that the indicated compression corresponds to a −10% or a −30% strain along the Z direction in figure 1(A).

The thickness of the actuation membrane (i.e. 800 μm) was optimised so that the device actuation pressure (i.e. the pressure necessary for the membrane to reach the bottom surface of the pillars, equal to 0.4 Atm and measured as previously described [34, 46]), depends only on the flexional rigidity of the membrane. It is not affected by the mechanical properties of the cell laden constructs, which can vary during the culture time.

The mechanically active platform reiterates a model that we developed to investigate mechanotransduction mechanisms in osteoarthritis [34, 47]. The pillars' T-like shape and the width of the space between them (30 μm) allow contact with the culture medium while preventing lateral expansion of the hydrogel upon compression, i.e. the achievement of confined compression (as we previously demonstrated using finite element simulations and experimental validations [34]). Such design was purposefully chosen to mimic the compressive strain field of the NP, where lateral expansion is hindered by the presence of the AF. Devices were fabricated in polydimethylsiloxane (PDMS, figure 1(D)). Thin sections of the device (figure 1(E)) were examined to confirm the differences in pillar heights between the 10% and 30% versions.

2.2. Hypoxia enhances maturation of NPoC constructs towards an NP-like phenotype

Interactions between NP cells and their surrounding ECM are essential for an effective transduction

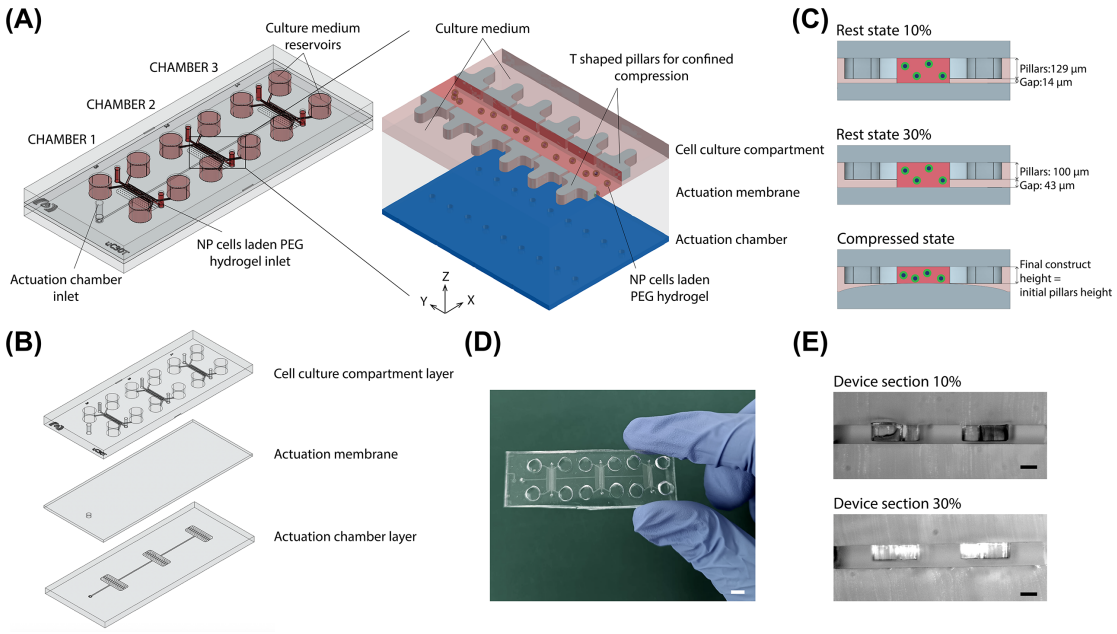

Figure 1. OoC device layout. (A) 3D schematic of the mechanically active device. The inset on the right illustrates the internal structure of the OoC. (B) 3D schematic illustrating the three PDMS layers composing the device. (C) Cross-sectional schematic of the device highlighting differences in pillars' height and gap size between the 10% and 30% configurations. The bottom diagram shows the device under compression, with the actuation membrane in contact with the bottom surface of the pillars. (D) Photograph of a fabricated device. Scale bar: 5 mm. (E) Examples of devices' cross-sections. Scale bar: 100 μm.

of mechanical signals from the extracellular environment to the intracellular one [19]. Thus, after having established the technological platform, we first aimed at obtaining microconstructs with gene expression levels and ECM composition resembling those of the native human NP tissue. Primary human NP cells from patients undergoing spinal surgery for lumbar disc degeneration were expanded in 2D, detached, and encapsulated in enzymatically cleavable polyethyleneglycole (PEG) hydrogels known to enable the formation of cartilaginous matrix by competent cells [34]. 3D NP cell-laden hydrogels were statically cultured within microscale devices for 14 d in differentiation medium (DM, see methods), under either normoxic or hypoxic conditions, the latter mimicking the oxygen tension experienced by NP cells *in vivo* [48, 49]. An outline of the experimental design is reported in figure 2(A).

NP cells cultured in both normoxia and hypoxia maintained a physiological round morphology and remained confined within the 3D culture space for the entire 14 d culture period (figure 2(B)). Quantitative reverse transcription polymerase chain reaction (RT-qPCR, figure 2(C)) revealed that on-chip differentiation of NP cells in both conditions led to a statistically significant increase in the expression of the NP ECM marker genes Collagen type II (*COL2A1*) and Aggrecan (*ACAN*). These increased up to 3 orders of magnitudes with respect to Day 0 controls and reached levels comparable to those of the native NP tissue. Specifically, we compared the gene expression levels of NPoC constructs to those of NP-cells harvested during an autopsy conducted on an elderly subject with no history of IDD. These cells (whose gene expression is indicated by the green band in figure 2(C)) were analysed immediately after extraction from their native tissue, without any expansion or conditioning, thus providing representative baseline levels of gene expression in human NPs.

To distinguish the assumption of an NP-like phenotype from hyaline-like chondrogenesis (which is also characterised by *COL2A1* and *ACAN* expression), we then evaluated the expression of the NP specific markers *CDH2* [25] and *OVOS2* [50–53]. Both normoxia and hypoxia induced an increase in *OVOS2* expression, reaching native-like levels (figure 2(C)). In contrast, *CDH2* expression in NPoC constructs cultured under hypoxia was closer to native levels (green band in figure 2(C)) than in constructs cultured under normoxia. *CDH2* encodes for the protein N-cadherin (NCAD), which is expressed by juvenile NP cells but whose expression decreases with aging and disease [25]. Culturing NPoC constructs in hypoxic conditions seemed therefore to result in a more mature phenotype.

Gene expression results on NP ECM markers were confirmed by immunofluorescence analyses. After 14 d of differentiation, NPoC constructs cultured both in normoxia and hypoxia showed substantial deposition of the NP matrix constituents COL2A1

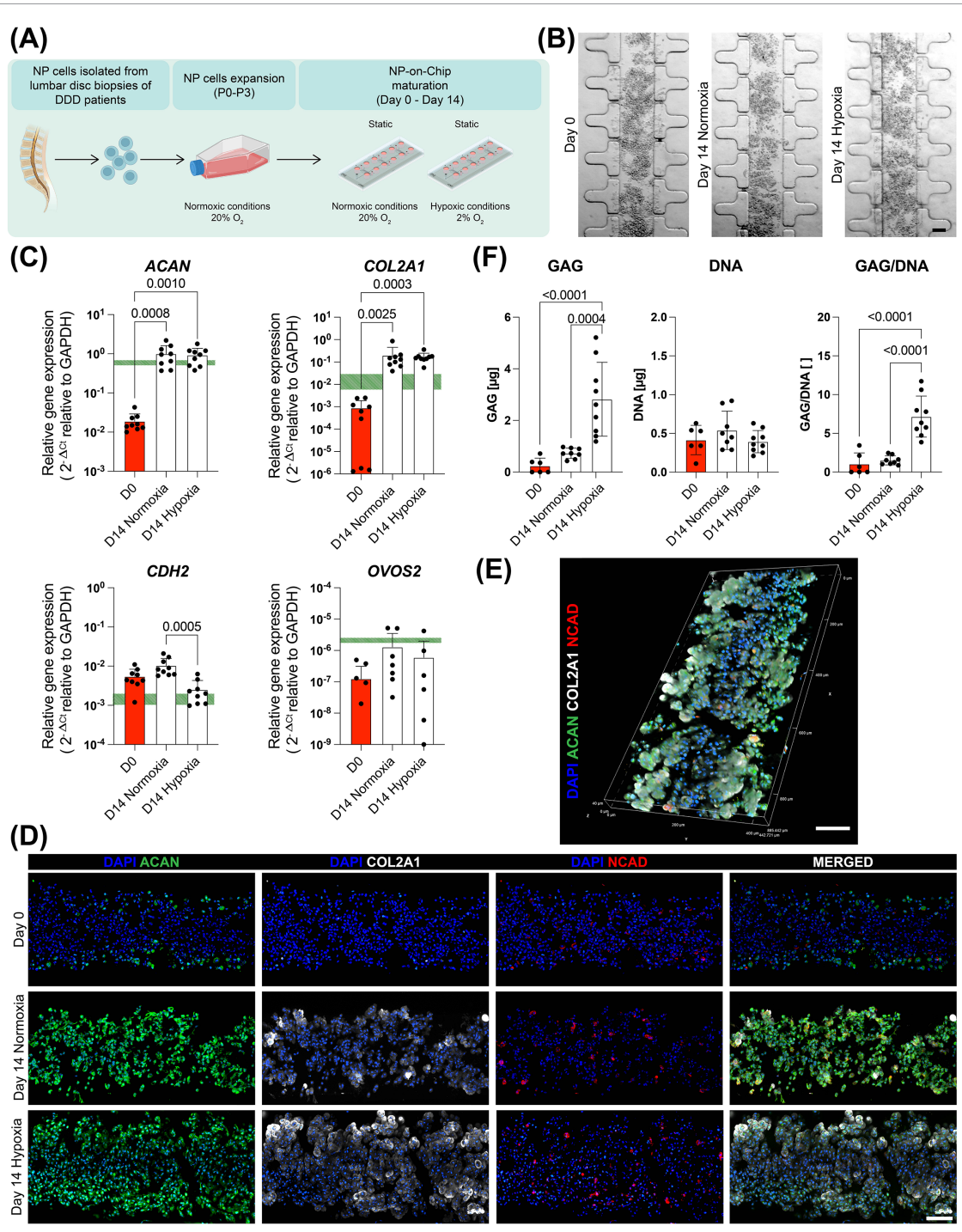

Figure 2. Maturation of NP-on-Chip (NPoC) constructs. (A) Schematic overview of experimental timeline and conditions. (B) Brightfield images of NPoC constructs at Day 0 (immediately after seeding into the OoC device) and after 14 d of static culture. Scale bar: 100 μm. (C) Quantification of gene expression in NPoC constructs via RT-qPCR ($N = 9$ independently cultured constructs from $N = 3$ donors). Statistical analysis was performed using the Kruskal–Wallis test with Dunn's post hoc test for multiple comparisons. Population normality was assumed if both Shapiro–Wilk and Kolmogorov–Smirnov tests returned positive results. Gene expression levels were normalised to GAPDH. Values are reported as mean + s.d. Adjusted p-values < 0.05 are indicated on the graph. Horizontal green bands represent the range of expression of native NP cells from a healthy human donor (i.e. without clinical history of IDD; $N = 3$ independently collected and measured samples from the same donor). (D) Representative immunofluorescence images (maximum intensity projections from confocal stacks) of NPoC constructs ($N = 9$ independently cultured constructs from $N = 3$ donors). Scale bar = 100 μm. (E) 3D confocal reconstruction of an NPoC construct cultured under hypoxia for 14 d. Scale bar = 100 μm. (F) Quantification of GAG content, DNA content, and their ratio in NPoC constructs ($N = 6$ from $N = 2$ donors at D0; $N \geqslant 8$ from $N = 3$ donors at D14). Statistical analysis was performed using ordinary one-way ANOVA with Tukey's multiple comparisons test for normally distributed data. Population normality was assessed using Shapiro–Wilk and Kolmogorov–Smirnov tests. p-values < 0.05 are reported on the graph. Values are presented as mean $\pm$ s.d. Created in BioRender. Martin, I. (2026) https://BioRender.com/qqa69j8

and ACAN, which was absent on Day 0 ((figure 2 (D), (E)). We also detected the presence of a number of small clusters of NCAD+ cells (figure 2(D)), as previously reported for *in vitro* cultured NP cells with elevated matrix synthesis and gene expression of NP-specific markers [25]. Despite the observed differences at the gene level (NCAD is encoded by *CDH2*) and slight variations in mean values, the number of NCAD+ cells/total number of cells did not show significant differences in NPoCs cultured under hypoxic or normoxic conditions and did not differ from Day 0 controls (mean ± s.d.: Day 0: 0.11 ± 0.11; Day 14 Normoxia: 0.12 ± 0.13; Day 14 hypoxia: 0.07 ± 0.15), possibly due to the high variability in NCAD+ cell numbers among samples (figure S2).

NPoC constructs cultured in hypoxia contained significantly higher levels of GAG than both Day 0 constructs and constructs cultured in normoxia (figure 2(F)). Hypoxia cultured NPoCs reached GAG/DNA ratios of 7.2 ± 2.6, compared to 1.5 ± 0.6 (for normoxia) and 1.0 ± 1.4 (Day 0 reference). Given the abundance of GAGs in the native matrix of healthy NP tissue, these results demonstrate that NPoCs' hypoxic differentiation supports the formation of microscale tissues with gene expression profiles and ECM composition more comparable to those of the native tissue. Consequently, the hypoxic condition was selected for subsequent loading experiments.

Of note, PDMS, the material adopted for fabricating the NPoC platform, is permeable to gases. Thus, the top surface of the NPoC construct is directly exposed to the oxygen concentration present in the incubator. This feature, united with the microscale dimensions of the NPoC constructs, allows to achieve a stricter control over the constructs' local oxygen tension with respect to commonly used NP models. To validate this concept, NP cells differentiation experiments were repeated using an established pellet model (i.e. 3D cellular aggregates) [46, 54]. The experimental procedure is detailed in figure S1(A). After 14 d of differentiation, pellets were stained with Safranin-O, to visualise their GAG content. Differently from NPoC constructs, normoxia promoted greater GAG accumulation, while hypoxia cultured pellets exhibited a loose matrix with dim Safranin-O positive stainings. Additionally, both culture conditions showed a necrotic core, which was more frequent and pronounced under hypoxic conditions (figure S1(B)). The results were consistent considering four NP human donors.

To determine whether these results depended on differences in oxygen concentration, we estimated the oxygen levels at the pellet surface and in their core under hypoxic and normoxic culture conditions using a simplified analytical model (see supplementary methods for details; figure S1(C)). Calculations indicated that the limited oxygen diffusion through the medium covering the pellets, together with the high cell density of the 3D aggregates, reduced oxygen concentrations at the pellet surface well below the incubator's theoretical levels. Within the core of hypoxia-cultured pellets, oxygen levels dropped to near zero, consistently with the formation of a necrotic core. Stable oxygen concentrations were instead predicted in the case of NPoC constructs using a similar analytical model (see supplementary methods), thus explaining observed differences in the deposition of ECM components.

Together, these findings demonstrate that NPoC constructs cultured under hypoxia achieve gene expression profiles and ECM compositions resembling those of native human adult tissue. They also highlight how the design and microscale dimensions of the NPoC model enable tighter control of critical experimental variables for the development of relevant human NP *in vitro* models.

2.3. Impact of simulated daily mechanical loading on NPoC constructs

In vivo, IVDs are continuously subjected to mechanical challenges whose cellular responses depend on the magnitude, frequency, pattern, and duration of the applied stimulus [44]. Physiological loading is known to promote NP's homeostasis by facilitating the transport of solutes, ensuring a correct balance between catabolic and anabolic cellular processes and suppressing inflammatory responses [55, 56]. On the other end, hyperphysiological mechanical stressors, such as heavy weight lifting, altered muscle activations, or lifestyle factors (e.g. vibration exposure, aberrant gait, or improper posture) may contribute to NP cell death, catabolism, and inflammation [12].

Within this framework, we aimed to assess whether the NPoC could recapitulate the mechanical responses observed in the NP under physiological and pathological conditions.

Firstly, by making use of the strain-controlled compression capabilities of the 10% and 30% versions of the device, we assessed if mature NPoC constructs (i.e. constructs cultured in hypoxia for 14 d, in static conditions) exhibited different responses to PC and HPC. Of note, our chosen value for the physiological compression, i.e. 10%, falls within the range of registered diurnal height variations in the lumbar discs of young non symptomatic adults [43], and it is slightly higher than reported disc compression levels in an *ex-vivo* human disc model [57].

NPoC constructs were exposed to cyclic loading (either PC or HPC) with a pattern of 1 h of stimulation and 1 h of rest over a 12 h daily period, for 7 consecutive days (figure 3(A)). Constructs cultured under static conditions for the entire period were used as controls. After 14 d of priming in hypoxia, cyclic loading was applied in normoxia (for both mechanically stimulated constructs and static controls). During

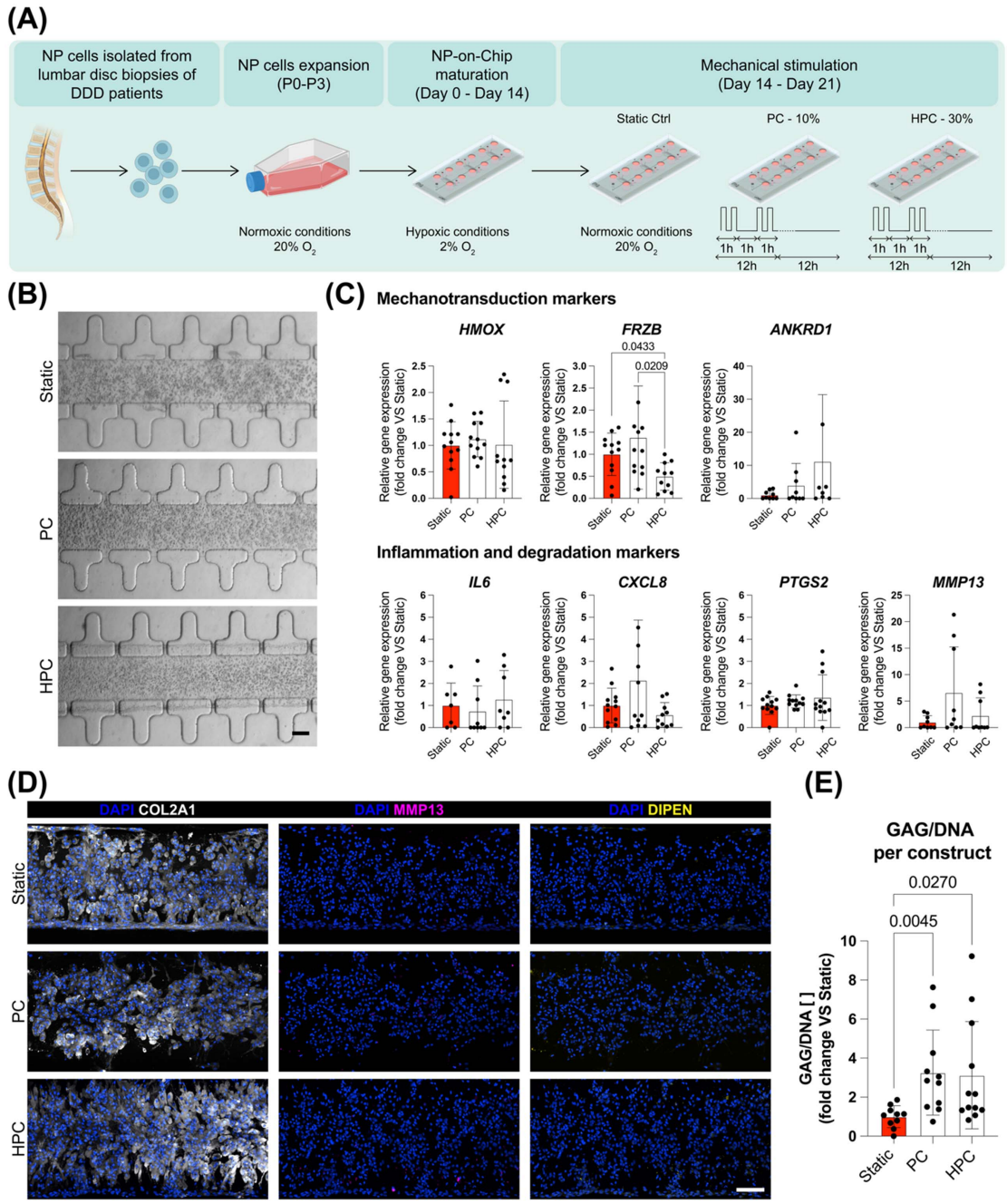

Figure 3. Impact of PC and HPC on NPoC constructs. (A) Schematic illustrating experimental timeline and conditions. (B) Brightfield images of mechanically stimulated and statically cultured NPoC constructs at Day 21. Scale bar: 100 μm. (C) Quantification of the effect of cyclic compression on NPoC constructs' gene expression via RT-qPCR ($N \geqslant 9$ independently cultured constructs from $N \geqslant 3$ donors). Statistics by Kruskal–Wallis test with Dunn's post hoc test for multiple comparisons. Populations' normality was assumed if both Shapiro–Wilk and Kolmogorov–Smirnov tests resulted positive. Expression levels of all genes were normalised to GAPDH expression; graphs show the fold change with respect to the average expression of static controls by donor. Values are reported as mean $\pm$ s.d. (adjusted) p-values < 0.05 are reported on the graph. (D) Representative immunofluorescence images of constructs subjected to static culture, PC, and HPC for 7 d (images from $N = 9$ independently cultured samples from $N = 3$ donors); scale bar = 100 μm. (E) Quantification of the effect of mechanical compression on GAG/DNA ratio ($N \geqslant 10$ independently cultured constructs from $N = 4$ donors). Statistics by Kruskal–Wallis test with Dunn's post hoc test for multiple comparisons. Populations' normality was assumed if both Shapiro–Wilk and Kolmogorov–Smirnov tests resulted positive. (Adjusted) p-values < 0.05 are reported on the graph. Values are reported as mean $\pm$ s.d. and represent the fold change relative to the average value of static controls for each donor. Created in BioRender. Martin (2026) https://BioRender.com/qqa69j8

IVD degeneration, native NPs are commonly subjected to vascular invasion, resulting in more elevated, non-physiological oxygen concentrations in the tissue. Therefore, all samples were cultured under normoxic conditions during the stimulation phase, to preserve possible oxygen-stress-mediated loading responses [58].

Neither PC nor HPC affected the overall morphology of NPoCs, with cells remaining round and evenly distributed within constructs (figure 3(B)). To detect

compression-level dependent effects, we investigated the gene expression of three mechanotransduction markers. While the expression of the putative mechanosensitive gene *HMOX* was not affected by PC and HPC, a compression-level dependent behaviour could be detected in the expression of the Wnt antagonist *FRZB*. The precise role of *FRZB* in IVD biology remains unclear; however, *FRZB* is known to be downregulated in a compression-dependent manner during osteoarthritis development in chondrocytes [34, 59] accordingly, we detected a decrease in the expression of *FRZB* only following HPC (figure 3(C)). We also detected an upward trend (i.e. an increase proportional to the applied compression level) in the expression of the YAP/TAZ and NF-kB target gene *ANKRD1*, which is known to be expressed by NP cells [60] and was demonstrated to be regulated by mechanical stimulation in other cell types [61–63]. The increase in expression of *ANKRD1* was however not significant and, while some samples highly responded to HPC, in others its expression remained at the baseline level.

Overall, these data indicate that NPoC constructs are sensitive to the magnitude of the applied cyclic compression. To determine if this response was translated into an IDD-like phenotype, we assessed the expression of the inflammatory and catabolic marker genes *IL6, CXCL8, PTGS2*, and *MMP13*.

No statistically significant effects of the tested PC and HPC regimens could be detected on inflammatory and catabolic mediators (figure 3(C)). The only changes were represented by a non-significant increase in the expression of *CXCL8* and *MMP13* upon PC. Since *MMP13* positivity could not be detected at the protein level (figure 3(D)), this finding may be attributed to a transient remodelling process activated by loading. Immunofluorescent imaging confirmed that neither PC nor HPC induced a degradative or catabolic effect ((figure 3(D)). NPoC constructs remained positive for COL2A1 and negative for MMP13 and DIPEN (a byproduct of aggrecan degradation by MMPs [64]), regardless of the applied mechanical stimulation. On the other end, both PC and HPC compression led to a significant increase in NPoC constructs' GAG content. Cyclically compressed constructs reached GAG/DNA ratios of (mean $\pm$ s.d.) 3.3 $\pm$ 2.2 (PC) and 3.1 $\pm$ 2.7 (HPC)) with respect to those of statically cultured controls (figure 3(E), non-normalised GAG, DNA, and GAG/DNA ratio are reported in figure S3).

Collectively, these results demonstrate that NPoC constructs respond to loading in a compression-dependent manner and suggest that, in our experimental setup, both PC and HPC exert an anabolic effect on GAG accumulation rather than indicating an IDD-inducing effect of HPC.

Of note, the DM used in our experimental setup contains dexamethasone, which, in addition to its positive effects on the expression of *COL2A1* and GAGs in chondrogenic differentiation protocols [65, 66], is a steroidal anti-inflammatory drug and may therefore have inhibited or masked some HPC-induced catabolic effects [67]. To avoid further interference with degradative processes, dexamethasone was removed from the DM during mechanical stimulation in subsequent experiments.

2.4. Sustained hyperphysiological compression induces hallmarks of IDD in NPoC constructs

IDD is linked to mechanical risk factors such as prolonged and/or strenuous activity, repeated exposure to vibrations, and chronic poor posture [8, 9]. Accordingly, we explored if mechanical overloading could trigger degenerative changes in the NPoC model.

To this aim, we assessed the effect of applying a 30% hyperphysiological compression with a regular daily routine, as done above (i.e. HPC:1 h on and 1 h off for 12 h), and with a prolonged stimulation, to mimic occupational hazards (i.e. sustained hyperphysiological compression, SHPC: continuous cyclical stimulation for 16 h,). Statically cultured constructs were used as controls.

To avoid masking mechanical overloading-induced degenerative responses, dexamethasone was omitted from the DM formulation during the stimulation phase. Interestingly, comparing static constructs cultured with and without dexamethasone, a significant increase in the expression of *MMP13* and *IL6* was detected for the latter (figure S4), highlighting that a baseline inflammation level might be active during the remodelling processes. Moreover, no *ANKRD1* expression could be detected in samples cultured without dexamethasone. Although not previously reported in IVD cells, this finding aligns with corticosteroid-induced modulation of *ANKRD1* [68, 69]. Static controls cultured without dexamethasone were therefore used as reference in subsequent experiments. The full experimental design is reported in figure 4(A).

While no differences in the constructs' overall appearance or cell morphology were evident in brightfield images (figure 4(B)), catabolic effects mediated by aberrant mechanical stimulation were observed in the gene expression of NPoCs. A significant reduction in *HMOX* expression was observed following SHPC, while *FRZB* expression was significantly downregulated following HPC (figure 4(C)). Moreover, both HPC and SHPC led to a significant increase in the expression of the degradative enzyme *MMP13*, and SHPC additionally upregulated the inflammatory mediator *PTGS2* (figure 4(C)). Upward trends were also observed in the expression of the inflammatory cytokines *IL6* and *CXCL8*, although these differences did not reach statistical significance, possibly due to the higher variability in the expression of these markers.

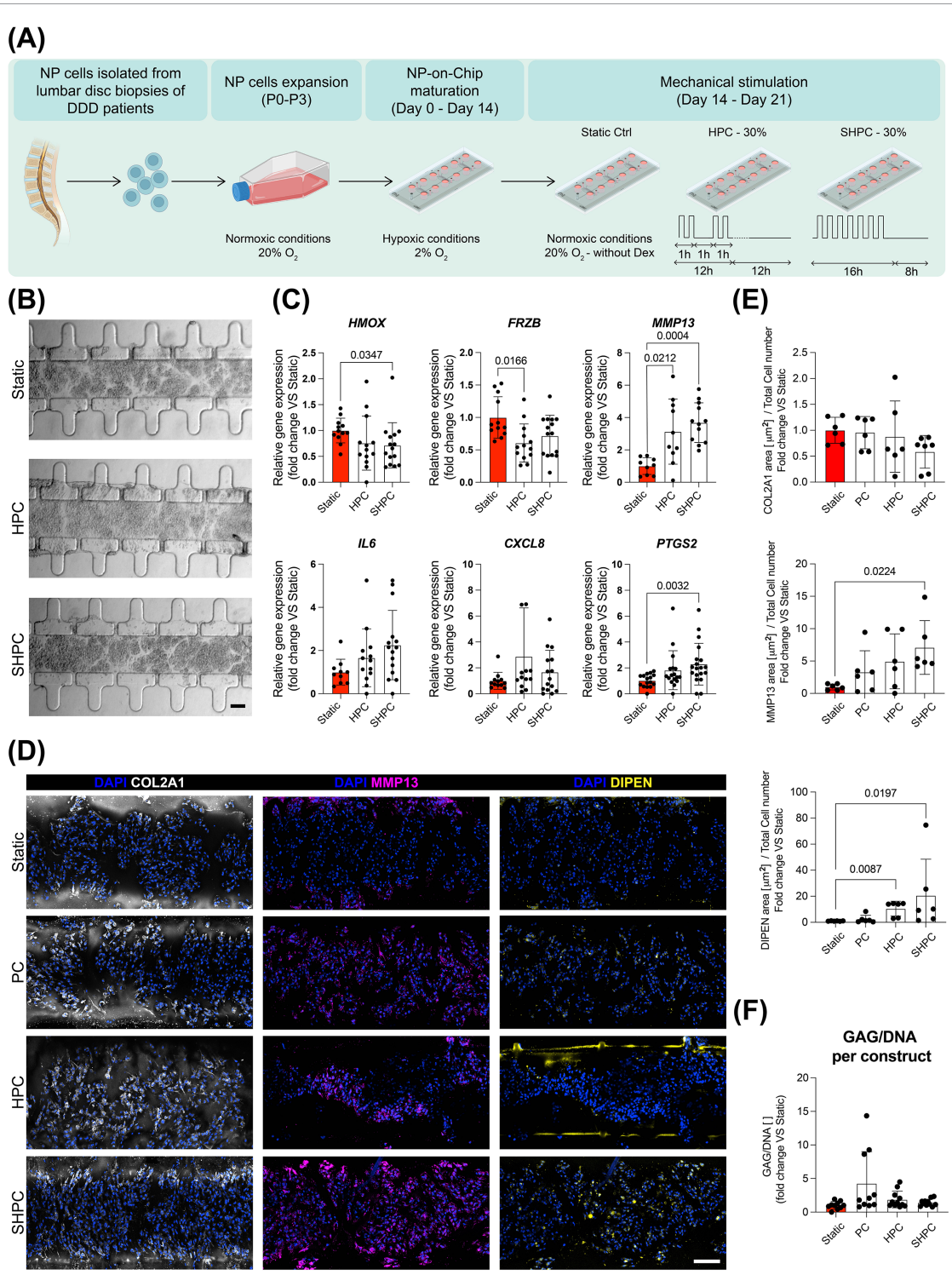

Figure 4. Mechanical stress induces IDD hallmarks in the NPoC model. (A) Schematic illustrating experimental timeline and conditions. (B) Brightfield images of mechanically stimulated and statically cultured NPoC constructs at Day 21. Scale bar = 100 μm. (C) RT-qPCR quantification of the effects of HPC and SHPC on NPoC constructs' gene expression ($N \geqslant 12$ independently cultured constructs from $N \geqslant 3$ donors). Statistical analysis by one-way ANOVA with Tukey's multiple comparison test for normally distributed data, and Kruskal–Wallis test with Dunn's multiple comparison test for non-normal data. Normality was assumed if both Shapiro–Wilk and Kolmogorov–Smirnov tests resulted positive. Adjusted p-values < 0.05 are reported on the graph. GAPDH was used as the housekeeping gene. Values are reported as mean ± s.d. and are represented as the fold changes relative to the average value of donor-specific static controls. (D) Representative immunofluorescence images of static controls and of constructs subjected to PC, HPC, and SHPC for 7 d (images from $N \geqslant 6$ independently cultured samples from $N = 3$ donors). Scale bar = 100 μm. (E) Quantification of COL2A1-, MMP13-, and DIPEN-positive areas in immunofluorescence images (images from $N \geqslant 6$ independently cultured samples from $N = 3$ donors). Statistical analysis by Kruskal–Wallis test with Dunn's post hoc test for multiple comparisons. Normality was assessed using both Shapiro–Wilk and Kolmogorov–Smirnov tests. Adjusted p-values < 0.05 are reported on the graph. Values are expressed as mean ± s.d. and represent fold changes relative to the average value of static controls for each donor. (F) Quantification of the effects of mechanical compression on the GAG/DNA ratio ($N \geqslant 10$ independently cultured constructs from $N = 4$ donors). Statistical analysis by Kruskal–Wallis test with Dunn's post hoc test for multiple comparisons. Normality was determined based on both Shapiro–Wilk and Kolmogorov–Smirnov tests. Adjusted p-values < 0.05 are reported on the graph. Values are expressed as mean ± s.d. and represent fold changes relative to the average value of donor-specific static controls. Created in BioRender. Martin, I. (2026) https://BioRender.com/qqa69j8

The mechanically induced activation of some catabolic processes was confirmed at the ECM level. Immunofluorescence imaging revealed that constructs subjected to both HPC and SHPC, while remaining rich in COL2A1, were positive for the degradative enzyme MMP13 and for the aggrecan degradation byproduct DIPEN [64] (figure 4(D)). Quantitative analysis (figure 4(E)) showed a significant increase in the DIPEN-positive area (normalised to total cell number) in HPC-stimulated samples compared to static controls, and a significant increase in both DIPEN and MMP13 positive areas in samples subjected to SHPC. These effects were not observed in constructs subjected to PC, indicating that the NPoC model effectively captures native-like responses to both physiological and pathological mechanical stimuli. No differences in the constructs cell numbers were observed quantifying the number of nuclei in analysed images (figure S5).

Finally, we evaluated the effect of the different compression regimens on the GAG accumulation in NPoC constructs (figure 4(F); Figure S6 reports raw GAG, DNA, and the non-donor normalised GAG/DNA ratio). In the absence of dexamethasone in the medium, only PC led to an increase (non-statistically significant) of the GAG/DNA ratio with respect to static controls (fold change, mean ± s.d.: 4.3 ± 4.7), while HPC (fold change, mean ± s.d.: 1.9 ± 1.2) and SHPC (fold change, mean ± s.d.: 1.4 ± 0.5) stimulated constructs remained at baseline levels.

Overall, these results confirm that the NPoC captures how hyper-physiological compression inhibits the matrix formation processes that happen at physiological regimens and demonstrate that, upon SHPC, it captures some of the early degradative and catabolic processes typical of IDD.

2.5. NPoC mechanically induced IDD traits are associated with increased apoptosis of NP cells

Following the onset of IDD traits through mechanical compression, we investigated if this phenotype was associated with the induction of apoptosis. We could not observe major macroscopic changes in cellular appearance or in the overall cell number following PC, HPC, and SHPC (figures 5(A) and S5). However, quantifying the number of cells expressing the apoptosis marker cleaved caspase 3 (Cc3), revealed a statistically significant increase in the number of Cc3+ cells in the SHPC condition with respect to both PC and static controls (figures 5(B) and (C)). The fold change of the Cc3+ cells/total cell number ratio with respect to static controls was (mean ± s.d.) 1.5 ± 1.1 for the PC condition, 2.2 ± 1.7 for the HPC condition, and 5.6 ± 2.9 for the SHPC condition.

Overall, these results demonstrate that excessive mechanical load alone is sufficient to trigger catabolic activity in a microscale human NP model, and that cyclic hyperphysiological compression sustained in time exacerbates the assumption of IDD-like traits through the induction of apoptosis.

This progression of degenerative events is consistent with histological observations of degenerated human IVDs, which frequently exhibit reduced cell density [70], further supporting the model's capability to capture physiologically relevant cellular responses.

2.6. Inhibition of TRPV4 partially attenuates IDD traits in NPoC constructs

Next, we performed a proof-of-concept validation of the capabilities of the NPoC model to be used as a drug screening platform.

Current IDD treatments rely primarily on anti-inflammatory compounds, such as corticosteroids [70]. Accordingly, supplementation of the culture medium with the corticosteroid dexamethasone—both prior to and during exposure of NPoC constructs to HPC (figure 3)—prevented the upregulation of *PTGS2* and *MMP13* that would otherwise be induced by aberrant mechanical stimulation (figure 4). Despite these anti-inflammatory effects, NPoC constructs subjected to HPC in the presence of dexamethasone still exhibited a decrease in the expression of *FRZB* (figure 3(C)), a Wnt pathway antagonist known to decrease in osteoarthritic cartilage proportionally to local tissue degradation [59]. While a direct correlation between *FRZB* and IDD has not been reported, IVD degeneration is known to depend on the alteration of Wnt signalling [71]. These observations suggest therefore that, in our model, mechanical loading influences Wnt signalling independently of inflammatory signalling, and that anti-inflammatory therapies may not affect these mechanosensing pathways.

Therefore, we tested whether inhibition of signalling downstream of the well-known mechanoresponsive, multimodal ion channel TRPV4 [13, 21] could reverse the IDD-like phenotype induced by aberrant mechanical loading in human NP cells.

The experimental timeline is depicted in figure 6(A). Mature NPoC constructs were obtained through 14 d of static differentiation in hypoxia and then subjected to 7 d of SHPC in normoxic conditions, to induce IDD traits. The SHPC regimen was subsequently maintained for further three days, during which NPoC constructs were either left untreated (vehicle only) or were treated with the TRPV4 antagonist GSK205 (10 μmol or 100 μmol). Constructs maintained under static conditions for the full 24 d served as controls.

No differences in constructs' overall appearance and cell morphology were detected in brightfield images (figure 6(B)). RT-qPCR (figure 6(C)) indicated that 10 μmol GSK205 had little effect on the mechanically induced degradative and inflammatory phenotype: *MMP13* expression remained unchanged,

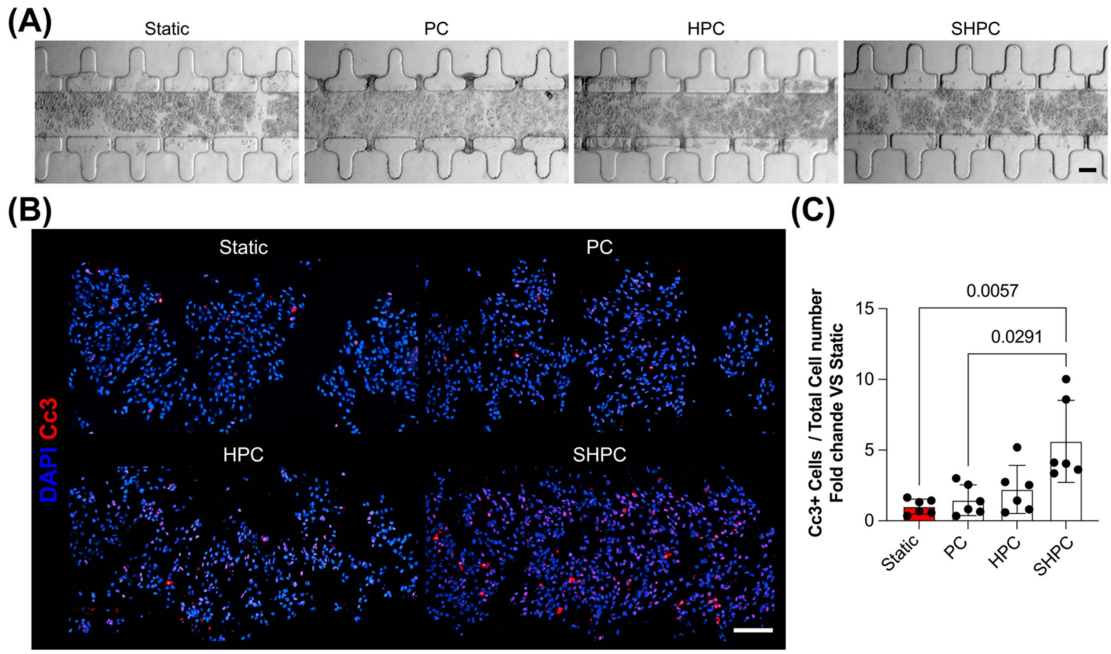

Figure 5. SHPC induces apoptosis in NPoC constructs (A) representative brightfield images of NPoC constructs at Day 21. Scale bar = 100 μm. (B) Representative confocal immunofluorescence images (maximum intensity projections) of constructs subjected to static culture, PC, HPC, and SHPC for 7 d (images from $N \geqslant 6$ independently cultured samples from $N = 3$ donors). Scale bar = 100 μm. (C) Quantification of Cc3+ cells (images from $N \geqslant 6$ independently cultured samples from $N = 3$ donors). Statistical analysis was performed using Kruskal–Wallis test with Dunn's post hoc test for multiple comparisons. Population normality was assessed using Shapiro–Wilk and Kolmogorov–Smirnov tests. (Adjusted) p-values < 0.05 are indicated on the graph. Values are reported as mean ± s.d. and represent fold changes relative to the average value of donor-specific static controls.

while *CXCL8* and *PTGS2* tended to increase. In contrast, treatment with 100 μmol GSK205 restored *MMP13* and *PTGS2* expression to levels similar to static controls' ones (set to 1 and indicated by the horizontal line in figure 6(C)). Furthermore, GSK205 promoted a dose-dependent increase in *FRZB* expression, that reached levels comparable to those of static controls at a concentration of 100 μmol.

Overall, these findings validate the NPoC as a suitable platform for screening anti-IDD compounds acting on mechano-dependent pathways, and suggest that inhibiting TRPV4-mediated aberrant mechanosensing may provide broader therapeutic benefits in reversing the pathological effects of IDD.

3. Discussion

Despite their potential to mimic the IVD microenvironment, current IVD-on-Chip models lack the ability to apply mechanical stimulation—crucial for homeostasis and a well-recognised risk factor for IDD.

To fill this gap, we engineered a new mechanically active NPoC model in which 3D constructs based on primary human cells can be exposed to controlled oxygen concentrations and subjected to either physiological (10%) or hyperphysiological (30%) cyclic compression under various regimens. Using this methodology, we generated NP-like microtissues with gene expression profiles and ECM composition akin to native counterparts and demonstrated that aberrant mechanical loading is sufficient to reproduce IDD traits in the model. Moreover, we provided a proof-of-concept that the platform is suitable for assessing the efficacy of 'mechano-targeting' pharmacological therapies.

Concerning the NPoC device, we adapted a proprietary OoC technology originally introduced to study the effect of aberrant mechanics on hyaline cartilage [34]. Featuring a cell culture compartment and a pneumatic actuation compartment, the device was designed to apply precise levels of confined compression to 3D constructs. Specifically, the T-shaped suspended pillars and their limited spacing provide sufficient contact area between the cellular constructs and the culture medium, while restricting lateral expansion under compression [34]. Such a strain field mimics the effect of loading on NPs *in vivo*, where lateral expansion is limited by the aligned collagen lamellae of the AF. This design was therefore specifically chosen to replicate the NP's strain upon compression with a reductionist approach.

Most existing macroscale IVD bioreactor studies use stress-controlled loading [10], where a fixed force is applied to macroscopic constructs or whole IVDs. These samples have variable mechanical properties, which results in nonuniform compression levels. In contrast, our device uses strain-controlled loading which depends exclusively on the device geometry. This ensures consistent control over the applied compression and allows distinction between the effects of

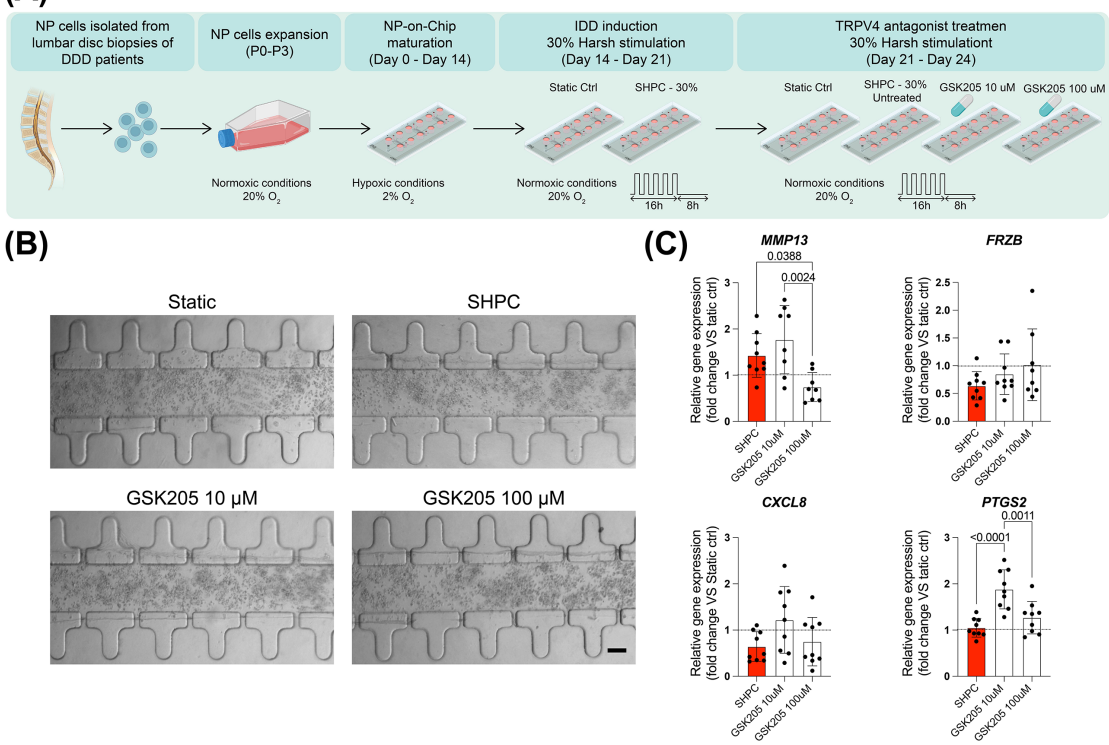

Figure 6. Inhibition of TRPV4 partially reverts IDD traits in the NPoC model. (A) Schematic of the experimental setup. NPoC constructs were cultured statically under hypoxic conditions for 14 d (differentiation phase), then subjected to SHPC for 7 d (IDD induction). Subsequently, constructs were exposed to the same compression regimen in the absence or presence of GSK205 (at 10 μmol and 100 μmol), for 3 d (treatment phase). During treatment (Day 21–24), both static controls and untreated samples received an equivalent concentration of vehicle as used in the GSK205 100 μmol condition. (B) Representative brightfield images of NPoC constructs on day 24. Scale bar = 100 μm. (C) RT-qPCR analysis of the effects of TRPV4 inhibition on gene expression in NPoC constructs ($N = 9$ independently cultured samples from a pool obtained mixing cells from $N = 3$ donors). Statistical analysis was performed using one-way ANOVA with Tukey's post-hoc test for normally distributed data and Kruskal–Wallis test with Dunn's multiple comparisons test for non-normal distributions. Normality was assumed when both Shapiro–Wilk and Kolmogorov–Smirnov tests resulted positive. Adjusted p-values < 0.05 are shown on the graph. GAPDH was used as the housekeeping gene. Data are presented as mean ± standard deviation and represent the fold change relative to the average value of static controls (indicated by the horizontal dotted line). Created in BioRender. Martin (2026) https://BioRender.com/qqa69j8

PC and HPC. Such precision is highly desirable for both mechanistic studies and drug screening applications. Furthermore, the NPoC enables an exponential increase in the number of experimental conditions that can be tested in a mechanically active setting. Given the platform's inner dimensions, twelve NPoC replicates can be obtained with 1×10^6 NP cells, as we verified during multiple experimental runs with the adopted seeding density of 50×10^6 cells ml_{PEG}^{-1}. Considering, roughly, a tenfold increase in cell number per passage and the feasibility of using cells up to passage three, more than ten thousand experimental replicates can be achieved starting from 10^6 cells, which is compatible with the cell number that can be retrieved from a single human disc during spine surgery procedures.

Concerning the maturation of NPoC tissues, hypoxic culture enhanced NP-like features compared to normoxia, confirming prior findings that low oxygen tension is crucial for maintaining the NP phenotype [72] and reinforcing the importance of mimicking the native hypoxic niche [25, 73]. Unlike mesoscale pellet cultures, which often develop non-physiological oxygen gradients, the NPoC platform ensures uniform oxygen exposure through its microscale geometry and PDMS gas permeability, enabling consistent NP-like differentiation. A recent spheroid-based study used AF cells to induce hypoxic conditions in the core of an NP cellular aggregate, achieving higher level of NP maturation while culturing cells in normoxia [42]. This approach is particularly suited for co-culture models replicating the oxygen tension level of the native IVD. However, the oxygen concentration in the NP core depends on the construct dimension, which may vary due to differences in the matrix deposition capacity of different donors. In our system, the oxygen tension is strictly regulated by imposed conditions and constructs' dimensions. Most existing IVD-related models lack this level of control [10, 36, 74], highlighting the NPoC as a promising platform for studying NP cell behaviour in a defined environment.

Of note, the NP cells used to obtain our NPoC model were isolated from degenerated IVDs (average Pfirrmann grade = 3.4 ± 1.1), which may retain features related to senescence and decreased anabolic

activity, and, as recently demonstrated, are constituted by populations with heterogeneous transcriptomic profiles [75]. However, patients' cells lose the expression of degeneration-associated cytokines and enzymes such as IL-1β, TNF-α, and MMPs when cultured under standard *in vitro* conditions, due to the removal of the native degradative microenvironment and pro-inflammatory signals. Both degenerated and healthy NP cells require an external stimulus to maintain or acquire an inflammatory or catabolic phenotype *in vitro*, with degenerated cells typically showing a stronger response. Overall, our data showed that the cells we used in our study retained the capacity of abundant synthesis of GAGs and *COL2A1*. Nevertheless, our findings should be interpreted with consideration that the degenerative baseline state may influence the cells anabolic and catabolic capacity and their responsiveness to mechanical compression.

Concerning the system's responses to mechanical stimulation, we confirmed that the NPoC model is sensitive to (i) the magnitude and (ii) the regimen of the applied compression, accurately replicating the native IVD's responses [12–14, 56].

A physiological 10% compression applied with a regimen simulating average daily activities stimulated anabolic processes, in line with previous research showing that physiological loading enhances NP cells' biosynthetic activity [76–78]. Conversely, a 30% HPC led to a downregulation of the Wnt signalling antagonist *FRZB*. The Wnt pathway is known to be involved in the formation, development, and degeneration of the IVD [71, 79], yet different aspects remain to be elucidated. *FRZB* was found to be downregulated in osteoarthritic hyaline cartilage [59], and we previously demonstrated a similar downregulation in a cartilage-on-chip model [34]. Thus, our present results indicate that the NPoC platform exhibits mechanosensitive behaviour consistent with known chondrocyte mechanobiology.

Notably, the decrease in *FRZB* expression occurred in the presence of the anti-inflammatory compound dexamethasone [80], added to the culture medium to promote chondrogenic and NP-like differentiation, which suppressed the upregulation of inflammatory/catabolic mediators induced by mechanical loading. This suggests that anti-inflammatory drugs alone may not fully address the mechanobiological basis of IDD and that our NPoC model is well-suited for studying early degeneration responses under anti-inflammatory interventions.

Upon removal of dexamethasone from the culture medium, HPC induced higher expression and deposition of catabolic and inflammatory markers, impaired ECM formation, and increased the number of apoptotic cells. These responses were further exacerbated by applying 30% compression in a daily regimen simulating strenuous, sustained hyperphysiological loading (i.e. SHPC). These results (i) confirm that mechanical loading alone is sufficient to elicit an IDD-like phenotype in the NPoC, and (ii) mirror established findings in human IVD degeneration, where prolonged exposure to repetitive stimuli (e.g. vibration from power tools) is a known IDD risk factor. Moreover, in the absence of dexamethasone, SHPC led to a reduction in *HMOX* expression, indicating a dysregulation of cytoprotective signalling pathways [71, 79, 81, 82]. While requiring further investigations, this result establishes a link between mechanical overloading and oxidative stress (i.e. *HMOX* downregulation), a well-known trigger of IDD [58].

Overall, these outcomes demonstrate the ability of our NPoC model to recapitulate mechanically induced features of IDD under highly controlled conditions, offering improved throughput and tissue mimicry compared with existing models that either fail to reproduce such phenotypes or lack the mechanistic insights enabled by the microscale control.

Lastly, we presented a proof-of-concept demonstrating the NPoC's potential for drug screening of compounds targeting mechanotransduction pathways.

TRPV4 is known to act on mechanotransduction by sensing transient changes in osmolarity [83]. As such, our NPoC platform is well-suited suited to assess its responses since the T-shaped geometry of the pillars prevents lateral expansion upon compression, thereby inducing a cyclical outflow and inflow of the incompressible interstitial fluid during stimulation. Given the high GAG content of NPoC constructs, this likely results in transient changes in osmolarity.

According with this hypothesis, we observed that the TRPV4 antagonist GSK205 mitigated the degradative and inflammatory phenotype induced by hyper-physiological compression, returning the gene expression of selected targets to levels similar to those of static controls. In addition, TRPV4 inhibition restored *FRZB* expression to its basal level, supporting the growing body of research indicating TRPV4 inhibition as a promising approach to address the mechanical triggers of IDD that anti-inflammatory drugs alone cannot target [13, 21, 22, 84, 85].

In this framework, a few limitations of the NPoC platform and of the study need to be addressed. Firstly, although we purposefully adopted a reductionist approach to isolate the effect of compression on NP cells, the IVD is naturally exposed to a complex range of mechanical stimuli, including flexion and torsion. Bioreactors for large tissue constructs and whole-organ IVD models can nowadays replicate movements with up to six degrees of freedom and allow continuous monitoring of multiple parameters [14]. Compared to these systems, the confined compression applied by our NPoC model constitutes an oversimplified approach. However, working at the microscale offers key benefits: it requires only small amounts of cells and reagents, removes

the need for animal-derived samples, and allows sufficient experimental replicates even with scarcely available human cells. Nevertheless, future IVD-on-Chip studies should explore more complex loading modalities—initially in isolation, and subsequently in combination—to better mimic *in vivo* conditions. Future studies should also better dissect the combinatorial effect of various compression levels (i.e. both PC and HPC) and the administration of compounds such as dexamethasone, during the IDD onset phase. Secondly, this study employed 50×10^6 cells ml_{PEG}^{-1}, which exceeds the native cellularity of the NP tissue. This concentration was chosen as a trade-off, to limit cell requirements while providing sufficient material for analyses such as RT-qPCR. Future research should investigate how different cell densities affect NP cells phenotype and behaviour. Thirdly, although PDMS, which was used to fabricate the device, is well-suited for enabling membrane flexion, owing to its hyperelastic properties, and for supporting oxygen diffusion, due to its gas permeability, it is also known to adsorb small lipophilic molecules [86]. Therefore, future drug screenings using the NPoC platform should incorporate protective coatings or apply concentration compensation strategies [87]. Lastly, to more accurately recapitulate the full biological complexity of the IVD's response to mechanical loading, additional compartments—such as the AFs and the cartilaginous endplates [88]—should be modelled and integrated, together with an assessment of the combinatorial effect of loading and pro-inflammatory cytokines, as previously done in different systems [89]. Furthermore, incorporating cells whose increased presence in the IVD microenvironment is associated with degeneration (e.g. sensory neurons, vascular cells, and immune cells) [90]) would enable the study of mechanical and therapeutic influences on vascular invasion and innervation, both of which are hallmarks of IDD progression.

4. Conclusion

We have developed a novel, human cell-based, mechanically active microscale NPoC platform that provides a 3D, NP-like microenvironment and responds to both homeostatic and hyperphysiological mechanical compression. The model captures cellular responses to biophysical cues, demonstrating that mechanical stress promotes inflammation and catabolism, whereas physiological loading preserves NP homeostasis. We validated that the system is responsive to both the magnitude and the regimen of the applied mechanical compression. The NPoC platform enables therefore precise and cost-effective mechanical stimulation of constructs exhibiting gene expression and ECM composition similar to native counterparts, while remaining compatible with standard laboratory workflows. Moreover, the NPoC has a higher experimental throughput than traditional macroscale bioreactors, supporting its future application in mechanobiology-driven drug screening campaigns. Such screening could elucidate key IDD mechanical drivers and accelerate the translation of potential disease-modifying drugs into clinical practice. Future developments will further enhance the model complexity by integrating additional IVD-relevant cell types.

5. Methods

5.1. Mechanically active microscale device design

The mechanically active, microscale OoC device features three identical culture chambers (figure 1(A)). Devices are composed of three layers: cell culture compartment, actuation membrane, and actuation chamber (figure 1(B)). Each cell culture chamber comprises a central channel (width 300 μm, height 143 μm), to host a cell-laden hydrogel, and lateral culture medium channels (width 450 μm, height 143 μm) connected to culture medium reservoirs. Channels are separated by two rows of suspended pillars with a T-shaped cross section. The shape of the pillars (each arm of the T measuring 100 μm in width and 300 μm in length, with a 30 μm gap between adjacent pillars) was optimised to resist outward bending and limit the lateral expansion of the gel in the central channel upon compression (i.e. to provide confined compression) [34]. Two versions of the device were developed, featuring pillar heights of 100 μm (30% version) and 129 μm (10% version), respectively. Beneath the culture chamber lies an unpatterned actuation membrane (thickness: 800 μm), which overlays the actuation chamber (height: 50 μm, width: 3340 μm). The actuation chamber includes four rows of widely spaced pillars (radius: 30 μm), introduced to prevent buckling. All three actuation compartments are connected to a single actuation inlet.

5.2. Mechanically active microscale device fabrication

Mechanically active OoC devices (figures 1(A) and (B)) were fabricated through PDMS (Sylgard 184, Dow corning) replica moulding. PDMS monomer and curing agent were mixed at a 10:1 weight-ratio and degassed at 10 mbar for 10 min. Culture chamber and actuation chamber were achieved pouring the PDMS mixture onto appropriately designed master moulds, which were obtained through photolithography of SU-8 photoresist onto 4-inch silicon wafers, as previously described [47]. The actuation membrane was realised using as mould a simple (unpatterned) silicon wafer, carefully controlling the amount of PDMS to obtain a final thickness of 800 μm. PDMS was cured for at least 2 h at 65 °C. Afterwards, it was removed from the master moulds, the outer shape of devices was trimmed using a razor

blade, and holes for hydrogel inlet and outlet (diameter, $D = 1$ mm), medium reservoirs ($D = 5$ mm), and actuation chamber ($D = 1.5$ mm) were bored using biopsy punchers. The final device was obtained exposing the 3 layers to air plasma (Harrick Plasma, Basic Plasma Cleaner) and bringing them in conformal contact for at least 30 min at 80 °C, to achieve irreversible bonding. Devices were sterilised through autoclaving and further cured at 70 °C for at least 24 h, to minimise the presence of possible leachates from uncured PDMS. Proprietary devices (uBeat® Compress Platform, BiomimX®) were produced under concession from BiomimX S.r.l.

5.3. Production of enzymatically cleavable polyethyleneglycole hydrogels

Cell-laden constructs were obtained embedding NP cells in a PEG hydrogel susceptible to cleavage from MMPs [91]. Briefly, 1 ml of FXIII (200 U ml^{-1}; Fibrogammin; CSL Behring) was activated with 100 μl of thrombin (20 U ml^{-1}; Sigma-Aldrich) for 30 min at 37 °C. The resulting activated FXIII (FXIIIa) was stored in small aliquots at −80 °C. Eight-arm PEG vinylsulfone (molecular weight: 40 kDa; NOF Europe) was functionalized with peptides containing either an FXIII glutamine acceptor substrate (Gln peptides; NQEQVSPL-ERCG-NH2; Bachem) or an MMP-degradable FXIII lysine donor substrate (Lys-MMPsensitive peptides; Ac-FKGGGPQGIWGQ-ERCG-NH2; Bachem), which resulted in 8-PEG-Gln or 8-PEG-MMPsensitive-Lys precursors, respectively. A stoichiometrically balanced solution of 8-PEG-Gln and 8-PEG-MMP sensitive-Lys was mixed in Tris buffer (50 mM Tris (pH 7.6)) and 50 mM calcium chloride for the indicated final dry mass content of hydrogel precursors, leaving a spare volume of 10% (v/v) for the addition of culture medium and cells. Hydrogel cross-linking was initiated by adding 10 U ml^{-1} of FXIIIa and by mixing vigorously. Hydrogels adopted throughout the study had a final concentration of 3% (v/v) PEG precursors and contained cells at a density of 50×10^6 cells $ml_{PEG}{}^{-1}$. Given the microscale dimensions of NPoC constructs, the cell density—higher than that of native adult human NP tissue—was optimised to ensure that sufficient cells could be obtained from each sample for analyses requiring minimal biological material while maintaining adequate throughput (e.g. DNA quantification and RT-qPCR).

5.4. Procurement, isolation, and expansion of NP cells

NP cells were harvested from donors ($n = 4$, 2 males, 2 females, average age = 49.5 ± 12 years old), undergoing spinal surgery for lumbar disc degeneration. Samples were obtained following approval of the local ethical committee (EKNZ-2015305, University Hospital Basel), after informed consent from the patients. The samples' degeneration level was graded using Pfirrmann scale [92] (average grade = 3.4 ± 1.1). NP tissue was separated from residual AF tissue using a scalpel, based on visual inspection by an experienced operator. The NP was then washed twice with phosphate buffered saline (PBS, Gibco), minced, and enzymatically digested (37 °C, 22 h) using 10 ml per g of tissue of a solution of 0.05% (w/v) type II collagenase (300 U mg^{-1}; Worthington Biochemical Corporation) in DMEM/F-12 (Sigma Aldrich, D8437) containing 5% (v/v) of foetal bovine serum (FBS). After the digestion, NP cells were passed through a 100 μm cell strainer (Fisher Scientific), washed, and resuspended in DMEM/F-12. Isolated NP cells were then counted using Trypan blue (Thermo-Fisher), plated in culture flasks at a density of 10^4 cells $cm^{-2,}$ and expanded (in a humidified incubator, 37 °C, 5% CO_2) in DMEM/F-12 (Sigma Aldrich, D8437) supplemented with 1 mM sodium pyruvate (Invitrogen), 100 U ml^{-1} penicillin, 100 μg ml^{-1} streptomycin, 0.29 mg ml^{-1} l-glutamine, 10% FBS, and 5 ng ml^{-1} fibroblast growth factor-2 (FGF-2), i.e. Expansion medium (EM). Cells were expanded up to 80% confluency before being replated. NP cells from different donors were expanded and used independently in all experiments, unless otherwise specified. Cells at passage three were adopted for on-chip experiments and 3D pellet cultures. Passaging causes NP cells to partially de-differentiate but it allows to achieve an adequate cell number and to reduce the inflammatory and catabolic signature of NP cells retrieved from IDD patients.

As a reference for the maturation of NPoC constructs, NP tissue from a lumbar disc of a cadaveric donor (male, 75 years old, with no reported history of IDD) was obtained after informed consent from the relatives, during routine autopsy procedures at the Department of Pathology of the University of Basel (ethical approval EKNZ-2023-02150). The full lumbar IVD was harvested and cut in half to expose the NP, estimating a degeneration grade of 2–3 on the Pfirrmann scale. The NP tissue was extracted with a scalpel and processed as described above. Cells were harvested from 3 different areas of the NP and digested separately. After enzymatic digestion, NP cells were dissolved in TRI reagent (T9424, Sigma Aldrich), to capture the *in vivo* gene expression as accurately as possible, and stored at −80 °C before being analysed through RT-qPCR.

5.5. Culture of NP 3D cell pellets

NP cells pellets were formed as we previously described [54, 93]. Briefly, passage three NP cells were detached using trypsin-EDTA (0.05%) (Thermo fisher, 25300096) and distributed in screw-top 1.5 ml Eppendorf tubes using 2.5×10^5 cells for each tube. Aggregation was obtained centrifuging the

Table 1. Mechanical stimulation regimens used for NPoC experiments.

Loading label	Compression level	Compression frequency	Compression regimen
Static control	None	None	None
Physiological compression (PC)	10%	1 Hz, 50% duty cycle;	1 h on, 1 h off for 12 h a day, for 7 d
Hyperphysiological compression (HPC)	30%	1 Hz, 50% duty cycle;	1 h on, 1 h off for 12 h a day, for 7 d
Sustained Hyperphysiological compression (SHPC)	30%	1 Hz, 50% duty cycle;	Continuous for 16 h a day, for 7 d

tubes at 1300 RPM for 3 min. Each tube was filled with 1 ml of DM. The adopted DM formulation, previously demonstrated to favour the maturation of NP-like 3D constructs *in vitro* [93], was composed by DMEM/F-12 (Sigma Aldrich, D8437) supplemented with 1 mM sodium pyruvate (Invitrogen, 11360-039), 100 U ml^{-1} penicillin, 100 μg ml^{-1} streptomycin, 0.29 mg ml^{-1} l-glutamine, 10 μg ml^{-1} Insulin–Transferrin–Selenium (Gibco, 51300-044), 0.56 mg ml^{-1} Linoleic acid (Sigma, L9530-5), 1.25 ml l^{-1} human serum albumin (CSL Behring, 43075), 10 ng ml^{-1} transform growth factor-beta 3 (TGF-β3) (100-36E, Peprotech), 0.1 μmol dexamethasone (Sigma, D-2915), and 0.1 mM ascorbic acid 2-phosphate (Sigma, A-8960). Tube caps were left partially open to allow oxygen exchange with the incubator atmosphere. Medium change was performed every 2 d. Pellets were cultured for 14 d either in normoxic (20% O_2) or in hypoxic (2% O_2) conditions in a humidified incubator (37 °C, 5% CO_2). An estimation of the oxygen concentration profile in 3D pellets was conducted through an analytical model, using the diffusion-advection equation. A full description of the adopted model is reported in supplementary methods.

5.6. NPoC constructs maturation

NPoC constructs were obtained embedding NP cells in the above-described PEG-based enzymatically cleavable hydrogel. Briefly, passage three NP cells were detached using trypsin-EDTA (0.05%) (Thermo fisher, 25300096), counted with Trypan blue (Thermo-Fisher), and incorporated as a single-cell suspension in the PEG hydrogel precursor solution, so to obtain a final cellular density of 50×10^6 cells $ml_{PEG}{}^{-1}$. The cell-polymer precursor solution was then mixed with 10 U ml^{-1} of thrombin activated factor FXIIIa and immediately manually injected into the central channel of microscale devices using a micropipette (Sarstedt, Sarpette ® M, single channel, 1–10 μl). After 10 min of incubation (37 °C, 5% CO_2), the lateral culture medium channels and reservoirs were filled with DM. The culture medium was changed every 3 d. Samples were cultured statically (i.e. with no mechanical stimulation) for 14 d, either in normoxic or in hypoxic conditions, in a humidified incubator (37 °C, 5% CO_2) before application of cyclic mechanical stimulation or collection for RT-qPCR, immunofluorescence imaging, or quantification of constructs' GAG and DNA content. Brightfield images of the constructs were acquired throughout the culture period.

5.7. NPoC mechanical stimulation

After 14 d of maturation, NPoC constructs were subjected to cyclic mechanical compression for 7 d, adopting compression levels and stimulation regimens reported in table 1. Cyclic loading (1 Hz, 50% duty cycle), either 10% compression (i.e. PC) or 30% compression (i.e. HPC), was applied with periods of 1 h of stimulation and 1 h of rest for 12 h a day, to mimic the periodic stimulation of daily activities. A second regimen where cyclic hyperphysiological compression was applied continuously for 16 h a day (i.e. SHPC) was introduced to mimic situations where the NP is continuously mechanically challenged (e.g. occupational hazards). Static culture constructs were used as controls.

Mechanical stimulation was achieved connecting OoC devices to a pressure regulator (Comnhas) linked to a custom-made electropneumatic controller able to apply the described loading regimens [34]. The entire setup was then connected to an upstream compressed air source. External connections were realised through Tygon tubing (Tygon ND 100-80, Cole Palmer, internal diameter: 0.5 mm). To prevent air from the pressure source to create bubbles, the actuation chamber was saturated with PBS filling the Tygon connection tubes with the liquid by applying a continuous low pressure (0.1 Atm) for 30 min. Cyclic stimulation was applied using a pressure of 0.4 Atm, which we previously demonstrated to be sufficient for the actuation membrane to reach the bottom surface of the pillars [33, 34]. The culture medium was changed every second day. Mechanical stimulation experiments were performed both with and without the presence of 0.1 μmol dexamethasone in the DM formulation. Both mechanically stimulated samples and static controls were cultured in normoxic conditions during the stimulation period.

5.8. TRPV4 inhibition

The NPoC model was tested as a drug screening tool by assessing the effect of inhibiting TRPV4-mediated signalling. NPoC constructs were cultured

Table 2. Genes targets of interest and corresponding molecular functions.

Gene	Abbreviation	Harmonised system (HS) code	Gene/product function
Aggrecan	*ACAN*	Hs00153936_m1	Proteoglycan, maintains NP hydration and absorbs compressive loading
Collagen type II	*COL2A1*	Hs00264051_m1	Provides structural support and tensile strength
Ovostatin 2	*OVOS2*	Hs02384746_g1	NP specific marker [50, 53]
N-Cadherin	*CDH2*	Hs00983056_m1	Encodes N-cadherin, a protein expressed by healthy NP cells whose expression decreases with aging and disease [25]
Hemeoxygenase I	*HMOX*	Hs01110250_m1	Regulates oxidative stress and prevents apoptosis influencing catabolic and anabolic processes; expression demonstrated to be regulated by mechanical loading ([58, 82, 94]
Frizzled-related protein	*FRZB*	Hs00173503_m1	Secreted Wnt antagonist, decreases following mechanical overloading [59]
Ankyrin repeat domain 1	*ANKRD1*	Hs00923600_m1	YAP/TAZ target, increases in response to mechanical loading [95, 96]
Interleukin 6	*IL6*	Hs00985639_m1	Active inflammation mediator
Interleukin 8	*CXCL8*	Hs00174103_m1	Active inflammation mediator
Cyclooxygenase 2	*PTGS2*	Hs00153133_m1	Mediator of active inflammation and pain responses; implicated in reactions to mechanical overloading *in vivo* [13]
Matrix metalloproteinase 13	*MMP13*	Hs00233992_m1	Matrix metalloproteinase involved in collagen degradation [5]

for 14 d in DM, in static conditions and hypoxic environment (maturation phase), then subjected to SHPC for further 7 d, in absence of dexamethasone and in normoxic conditions (IDD induction phase). Following the IDD induction period, constructs were treated with the TRPV4 antagonist GSK205 (MedChemExpress, HY-120691A, molecular formula $C_{24}H_{25}BrN_4S$) using dimethyl sulphoxide (DMSO, Sigma Aldrich, D2650) as a vehicle. GSK205 was administered either at 10 μmol, previously demonstrated to protect mouse IVDs from loading induced degeneration [21], and at 100 μmol, to investigate dose dependent effects and compensate for possible adsorption from PDMS, which is known to adsorb small lipophilic molecules. During the drug treatment, constructs were still exposed to SHPC and were conditioned with DM without TGF-β3 and dexamethasone. Untreated controls were exposed to the same vehicle concentration as used in the TRPV4 100 μmol condition. Static controls cultured under the same conditions were used as reference.

5.9. Gene expression analysis

Total RNA was extracted using TRI reagent® (T9424, Sigma Aldrich), according to the manufacturer instructions. Glycerol (G5516, Sigma-Aldrich) was employed to enhance RNA precipitation. Reverse transcription and complementary DNA (cDNA) synthesis were performed using the SuperScript III Reverse Transcriptase Kit (18080093, Invitrogen). RT-qPCR was performed according to standard protocols, using the Applied Biosystems 7300 Real-Time PCR system and equalising the amount of cDNA present in each reaction well. Genes of interest, reported in table 2, were analysed using the corresponding TaqMan Gene Expression Assays (Applied Biosystems). *GAPDH* (Hs02758991_g1) was used as housekeeping gene given its expression stability within our experimental conditions.

5.10. GAG and DNA quantification

The amount of GAG and DNA contained in NPoC constructs was quantified through biochemical analyses. Cellular constructs were extracted from microscale devices by peeling off the actuation chamber and actuation membrane layers and scraping the constructs with a 200 μl pipet tip. Constructs were digested (overnight, 56 °C) in a solution of proteinase-K (1 mg ml^{-1} proteinase-K in 50 mM Tris buffer supplemented with 1 mM EDTA, 1 mM iodoacetamide, and 10 μg ml^{-1} pepstatin-A), using 500 μl of solution per construct/pellet. GAG amounts were measured spectrophotometrically, after reaction with dimethylmethylene blue, using the Blyscan™ Sulphated GAG Assay Kit (Biocolor). Solutions with known concentrations of chondroitin sulphate were used to generate a calibration curve. DNA was quantified using the CyQuant™ Cell Proliferation Assay Kit (Molecular Probes, Eugene, OR) according to the manufacturer's instructions. Both measurements were performed

with a configurable multimode microplate reader (Synergy H1, BioTek Instruments).

5.11. Immunofluorescence staining and analyses

Immunofluorescence stainings were performed on NPoC constructs at Day 0, Day 14, and Day 21, directly within OoC devices. Samples were washed with PBS and fixed overnight at 4 °C in 4% (v/v) paraformaldehyde. Actuation membrane and chamber layers were then peeled off to expose the cellular constructs. Cell-laden hydrogels were permeabilised with a 0.5% (v/v) solution of Triton X (Sigma-Aldrich). Non-specific binding was blocked with a solution of 0.3% (v/v) Tween 20 (Sigma-Aldrich) and 3% (v/v) goat serum in PBS (1 h, room temperature).

Primary antibodies were diluted in the blocking solution and incubated overnight at 4 °C: Aggrecan (ACAN, Abcam, ab1864141, dilution 1:200), collagen type II (COL2A1, Abcam, ab185430, dilution 1:200), and N-cadherin (NCAD, BD Biosciences, 610920, dilution 1:200) were used to study constructs' differentiation; matrix metalloproteinase 13 (MMP13, Abcam, ab39012, dilution 1:2000), DIPEN (a C-terminal aggrecan fragment generated by MMPs cleavage [64], MD Bioproducts, 1042002, dilution 1:200), and (Cc3, Cell Signalling, 9661, dilution 1:100) were used to assess the effects of PC, HPC, ad SHPC. After incubation with primary antibodies, samples were washed with the blocking solution (20 min at room temperature, the operation was repeated twice) and subsequently incubated for 1 h at room temperature with secondary antibodies labelled with Alexa Fluor 488, Alexa Fluor 546, and Alexa Fluor 647 (Invitrogen, dilution 1:200), as appropriate. Staining with 4′,6-diamidino-2-phenylindole (DAPI) was used to identify cell nuclei.

Confocal imaging was performed using a Nikon AxR confocal microscope. Image analysis was conducted using ImageJ and QuPath [97] software. Maximum intensity projections of confocal stacks were generated in ImageJ and used for image quantification in QuPath. The total number of cells was computed using the QuPath cell detection tool. Staining-positive areas and staining-positive cells were identified using threshold-based pixel and object classifiers, respectively.

5.12. Safranin-O/fast green histological stainings

NP cells pellets were washed with PBS, fixed in 4% paraformaldehyde overnight at 4 °C, dehydrated, and embedded in paraffin. 5 μm thick sections of the samples were cut through a microtome (Microm HM 340E). Subsequently, sections were deparaffinised, rehydrated, and stained with Safranin-O (Saf-O, Sigma 84120) according to standard protocols, to visualise the GAG content. Fast green (Sigma-Aldrich: F-7252) was used as counter staining for collagen; haematoxylin (Papanicolaou J.T. BAKER: 3873) was adopted as a nuclear staining. Histological sections were imaged using a Nikon, Eclipse Ti2 microscope with a Nikon DS-Ri2 camera.

5.13. Statistical analysis

Results of biochemical analyses and image quantifications are presented as mean ± standard deviation. RT-qPCR results are presented as mean + standard deviation when reporting the relative gene expression with respect to GAPDH ($2^{-\Delta Ct}$), and as mean ± standard deviation when reporting the fold change with respect to a control condition ($2^{-\Delta\Delta Ct}$). Single data were plotted to account for non-normal distributions. Population normality was verified using Shapiro–Wilk and Kolmogorov–Smirnov tests. Non-paired double comparisons were performed using two tailed *t*-test for normal populations and Mann–Whitney test for non-Gaussian ones. Multiple comparisons were performed using one-way analysis of variance (ANOVA) followed by Tukey's post hoc test for normally distributed data and Kruskal–Wallis test followed by Dunn's post hoc test for non-normal data.

Data availability statement

All data that support the findings of this study are included within the article (and any supplementary files).

Supporting methods and data available at https://doi.org/10.1088/1758-5090/ae3d85/data1.

Acknowledgments

The authors are grateful to the University of Basel Histology Core Facility for the support with stainings, and to Professor Alexandar Tzankov, Head of the Department of Histopathology and Autopsy at the Institute of Medical Genetics and Pathology at University Hospital Basel, for his contribution in providing the autopsy IVD sample. The silicon wafer micropatterning was performed at PoliFAB, the micro- and nanofabrication facility of Politecnico di Milano. The device design was kindly provided by BiomimX S.r.l. The authors are particularly grateful to Professor Paola Occhetta for her constructive comments. This work was partially funded by the Swiss National Science Foundation (Grant Number 310030_175660/1), by the Centre for Applied Biotechnology and Molecular Medicine (CABMM) (Grant Numbers 05/2021), and by the European Research Council (ERC) under the European Union's Horizon 2020 research and innovation program (Grant Agreement No. 810111-EpiCrest2Reg). Schemes in figures were generated using BioRender.com, Autodesk AutoCAD, and Autodesk Fusion360.

Created in BioRender. Martin (2026) https://BioRender.com/psrcygq.

Conflict of interest

All authors declare they have no conflict of interests.

Ethical statement

Nucleus pulposus cells used in this study were obtained either from patients undergoing spinal surgery at the University Hospital of Basel or from routine autopsy procedures performed at the Department of Pathology, University Hospital of Basel. All samples were collected with the approval of the local ethics committee (EKNZ-2015 305 and EKNZ-2023-02150), under the general consensus of the University Hospital of Basel, and after informed consent of the patients or their relatives. Donors' material was adequately anonymised and no personal information from the patients was retained.

This study was conducted in accordance with the principles embodied in the Declaration of Helsinki and in accordance with local statutory requirements.

Author contributions

Olga Krupkova 0000-0002-2041-8557
Conceptualization (equal), Funding acquisition (equal), Investigation (supporting), Project administration (supporting), Supervision (equal), Writing – original draft (equal), Writing – review & editing (supporting)

Bianca Aterini 0009-0008-0963-8365
Formal analysis (supporting), Investigation (supporting), Methodology (supporting)

Nader Rahal 0009-0005-2238-8426
Methodology (supporting)

Elias Schulze
Methodology (supporting), Resources (supporting)

Salim Darwiche 0000-0001-5116-4564
Methodology (supporting), Resources (supporting)

Martin Ehrbar 0000-0003-2707-4870
Methodology (supporting), Resources (supporting), Writing – review & editing (supporting)

Karoliina Pelttari 0000-0002-3547-1879
Conceptualization (supporting), Funding acquisition (supporting), Project administration (equal), Writing – original draft (supporting), Writing – review & editing (supporting)

Ivan Martin 0000-0001-6493-0432
Conceptualization (supporting), Funding acquisition (supporting), Project administration (supporting), Writing – original draft (supporting), Writing – review & editing (supporting)

Stefan Schären
Project administration (supporting), Resources (supporting)

Arne Mehrkens 0000-0002-9189-4278
Conceptualization (supporting), Funding acquisition (equal), Project administration (supporting), Resources (equal), Supervision (supporting), Writing – original draft (supporting), Writing – review & editing (supporting)

Andrea Barbero 0000-0001-5252-789X
Conceptualization (supporting), Funding acquisition (supporting), Project administration (supporting), Resources (equal), Supervision (equal), Writing – original draft (supporting), Writing – review & editing (supporting)

Andrea Mainardi 0000-0001-8228-6441
Conceptualization (lead), Data curation (lead), Formal analysis (lead), Funding acquisition (supporting), Investigation (lead), Methodology (lead), Project administration (supporting), Resources (equal), Supervision (equal), Validation (lead), Visualization (lead), Writing – original draft (lead), Writing – review & editing (equal)

References

[1] Foster N E *et al* 2018 Prevention and treatment of low back pain: evidence, challenges, and promising directions *Lancet* **391** 2368–83
[2] Fatoye F, Gebrye T, Ryan C G, Useh U and Mbada C 2023 Global and regional estimates of clinical and economic burden of low back pain in high-income countries: a systematic review and meta-analysis *Front. Public Health* **11** 1098100
[3] Zhang Y, Guo T-M, Guo X and Wu S-X 2009 Clinical diagnosis for discogenic low back pain *Int. J. Biol. Sci.* **5** 647–58
[4] Jiang W *et al* 2023 Intervertebral disc human nucleus pulposus cells associated with back pain trigger neurite outgrowth *in vitro* and pain behaviors in rats *Sci. Transl. Med.* **15** eadg7020
[5] Binch A L A, Fitzgerald J C, Growney E A and Barry F 2021 Cell-based strategies for IVD repair: clinical progress and translational obstacles *Nat. Rev. Rheumatol.* **17** 158–75
[6] Zhang Y, Sun Z, Liu J and Guo X 2008 Advances in susceptibility genetics of intervertebral degenerative disc disease *Int. J. Biol. Sci.* **4** 283–90
[7] Chan S C W, Ferguson S J and Gantenbein-Ritter B 2011 The effects of dynamic loading on the intervertebral disc *Eur. Spine J.* **20** 1796–812
[8] Macedo L G and Battié M C 2019 The association between occupational loading and spine degeneration on imaging-a systematic review and meta-analysis *BMC Musculoskelet. Disord.* **20** 489
[9] Adams M A and Roughley P J 2006 What is intervertebral disc degeneration, and what causes it? *Spine* **31** 2151–61
[10] Mainardi A, Cambria E, Occhetta P, Martin I, Barbero A, Schären S, Mehrkens A and Krupkova O 2021 Intervertebral disc-on-a-chip as advanced *in vitro* model for mechanobiology research and drug testing: a review and perspective *Front. Bioeng. Biotechnol.* **9** 826867
[11] Sadowska A, Kameda T, Krupkova O and Wuertz-Kozak K 2018 Osmosensing, osmosignalling and inflammation: how

intervertebral disc cells respond to altered osmolarity *Eur. Cells Mater.* **36** 231–50
[12] Fearing B V, Hernandez P A, Setton L A and Chahine N O 2018 Mechanotransduction and cell biomechanics of the intervertebral disc *JOR Spine* **1** e1026
[13] Cambria E, Heusser S, Scheuren A C, Tam W K, Karol A A, Hitzl W, Leung V Y, Müller R, Ferguson S J and Wuertz-Kozak K 2021 TRPV4 mediates cell damage induced by hyperphysiological compression and regulates COX2/PGE2 in intervertebral discs *JOR Spine* **4** e1149
[14] Pfannkuche J-J, Guo W, Cui S, Ma J, Lang G, Peroglio M, Richards R G, Alini M, Grad S and Li Z 2019 Intervertebral disc organ culture for the investigation of disc pathology and regeneration—benefits, limitations, and future directions of bioreactors *Connect. Tissue Res.* **61** 304–21
[15] Mwale F, Roughley P, Antoniou J, Alini M, Hollander A, Kirsch T and Stokes I 2004 Distinction between the extracellular matrix of the nucleus pulposus and hyaline cartilage: a requisite for tissue engineering of intervertebral disc *Eur. Cell. Mater.* **8** 58–64
[16] He R *et al* 2021 HIF1A Alleviates compression-induced apoptosis of nucleus pulposus derived stem cells via upregulating autophagy *Autophagy* **17** 3338–60
[17] Gawri R, Rosenzweig D H, Krock E, Ouellet J A, Stone L S, Quinn T M and Haglund L 2014 High mechanical strain of primary intervertebral disc cells promotes secretion of inflammatory factors associated with disc degeneration and pain *Arthritis Res. Ther.* **16** R21
[18] McNally D S and Adams M A 1992 Internal intervertebral disc mechanics as revealed by stress profilometry *Spine* **17** 66–73
[19] Fearing B V *et al* 2019 Mechanosensitive transcriptional coactivators MRTF-A and YAP/TAZ regulate nucleus pulposus cell phenotype through cell shape *FASEB J.* **33** 14022–35
[20] Kameda T *et al* 2019 Expression and activity of TRPA1 and TRPV1 in the intervertebral disc: association with inflammation and matrix remodeling *Int. J. Mol. Sci.* **20** 1767
[21] Easson G W D, Savadipour A, Anandarajah A, Iannucci L E, Lake S P, Guilak F and Tang S Y 2023 Modulation of TRPV4 protects against degeneration induced by sustained loading and promotes matrix synthesis in the intervertebral disc *FASEB J.* **37** e22714
[22] Cambria E, Arlt M J E, Wandel S, Krupkova O, Hitzl W, Passini F S, Hausmann O N, Snedeker J G, Ferguson S J and Wuertz-Kozak K 2020 TRPV4 inhibition and CRISPR-Cas9 knockout reduce inflammation induced by hyperphysiological stretching in human annulus fibrosus cells *Cells* **9** 1736
[23] Wang Y, Bai B, Hu Y, Wang H, Liu N, Li Y, Li P, Zhou G and Zhou Q 2021 Hydrostatic pressure modulates intervertebral disc cell survival and extracellular matrix homeostasis via regulating hippo-YAP/TAZ pathway *Stem Cells Int.* **2021** 1–17
[24] Fusellier M, Clouet J, Gauthier O, Tryfonidou M, Le Visage C and Guicheux J 2020 Degenerative lumbar disc disease: *in vivo* data support the rationale for the selection of appropriate animal models *Eur. Cell. Mater.* **39** 18–47
[25] Hwang P Y *et al* 2016 N-cadherin is key to expression of the nucleus pulposus cell phenotype under selective substrate culture conditions *Sci. Rep.* **6** 28038
[26] Molladavoodi S, McMorran J and Gregory D 2019 Mechanobiology of annulus fibrosus and nucleus pulposus cells in intervertebral discs *Cell Tissue Res.* **379** 429–44
[27] Carmagnola I, Di Torino P, Bo Zhao I, Cambria E, Brunner S, Heusser S, Fisch P, Hitzl W, Ferguson S J and Wuertz-Kozak K 2020 Cell-laden agarose-collagen composite hydrogels for mechanotransduction studies *Front. Bioeng. Biotechnol.* **8** 589223
[28] Esch E W, Bahinski A and Huh D 2015 Organs-on-chips at the frontiers of drug discovery *Nat. Rev. Drug Discov.* **14** 248–60
[29] Bhatia S N and Ingber D E 2014 Microfluidic organs-on-chips *Nat. Biotechnol.* **32** 760–72
[30] Xia Y and Whitesides G M 1998 Soft lithography *Annu Rev. Mater. Sci.* **28** 153–84
[31] Occhetta P, Centola M, Tonnarelli B, Redaelli A, Martin I and Rasponi M 2015 High-throughput microfluidic platform for 3D cultures of mesenchymal stem cells, towards engineering developmental processes *Sci. Rep.* **5** 1–12
[32] Visone R, Ugolini G S, Cruz-Moreira D, Marzorati S, Piazza S, Pesenti E, Redaelli A, Moretti M, Occhetta P and Rasponi M 2021 Micro-electrode channel guide (μECG) technology: an online method for continuous electrical recording in a human beating heart-on-chip *Biofabrication* **13** 035026
[33] Mainardi A, Carminati F, Ugolini G S, Occhetta P, Isu G, Robles Diaz D, Reid G, Visone R, Rasponi M and Marsano A 2021 A dynamic microscale mid-throughput fibrosis model to investigate the effects of different ratios of cardiomyocytes and fibroblasts *Lab Chip* **21** 4177–95
[34] Occhetta P, Mainardi A, Votta E, Vallmajo-Martin Q, Ehrbar M, Martin I, Barbero A and Rasponi M 2019 Hyperphysiological compression of articular cartilage induces an osteoarthritic phenotype in a cartilage-on-a-chip model *Nat. Biomed. Eng.* **3** 545–57
[35] McKinley J P and O'Connell G D 2024 Review of state-of-the-art micro and macro-bioreactors for the intervertebral disc *J. Biomech.* **165** 111964
[36] Tavakoli J, Diwan A D and Tipper J L 2023 Intervertebral disc-on-a-chip: a precision engineered toolbox for low back pain studies *Trends Biotechnol.* **41** 1339–42
[37] Hwang M H, Son H-G, Kim J and Choi H 2020 *In vitro* model of distinct catabolic and inflammatory response patterns of endothelial cells to intervertebral disc cell degeneration *Sci. Rep.* **10** 1–13
[38] Dai J *et al* 2019 Microfluidic disc-on-a-chip device for mouse intervertebral disc—pitching a next-generation research platform to study disc degeneration *ACS Biomater. Sci. Eng.* **5** 2041–51
[39] Xie W *et al* 2023 Intervertebral Disc-on-a-Chip^{MF}: a new model for mouse disc culture via integrating mechanical loading and dynamic media flow *Adv. Mater. Technol.* **8** 2300606
[40] Chou P H, Wang S T, Yen M H, Liu C L, Chang M C and Lee O K S 2016 Fluid-induced, shear stress-regulated extracellular matrix and matrix metalloproteinase genes expression on human annulus fibrosus cells *Stem Cell Res Ther.* **7** 1–8
[41] Shin J *et al* 2019 Electrical impulse effects on degenerative human annulus fibrosus model to reduce disc pain using micro-electrical impulse-on-a-chip *Sci. Rep.* **9** 1–11
[42] Kim T-W, Kim A-G, Hwang M-H and Choi H 2025 Intervertebral disc spheroids as an *in vitro* multicellular platform for recapitulating the microenvironment of intervertebral disc degeneration *Biofabrication* **17** 035023
[43] Martin J T, Oldweiler A B, Kosinski A S, Spritzer C E, Soher B J, Erickson M M, Goode A P and DeFrate L E 2022 Lumbar intervertebral disc diurnal deformations and T2 and T1rho relaxation times vary by spinal level and disc region *Eur. Spine J.* **31** 746–54
[44] Sowa G, Coelho P, Vo N, Bedison R, Chiao A, Davies C, Studer R and Kang J 2011 Determination of annulus fibrosus cell response to tensile strain as a function of duration, magnitude, and frequency *J. Orthop. Res.* **29** 1275–83
[45] Li P, Hou G, Zhang R, Gan Y, Xu Y, Song L and Zhou Q 2017 High-magnitude compression accelerates the premature senescence of nucleus pulposus cells via the p38 MAPK-ROS pathway *Arthritis Res. Ther.* **19** 1–14
[46] Mainardi A *et al* 2025 An organ-on-chip platform for strain-controlled, tissue-specific compression of cartilage and mineralized osteochondral interface to study mechanical overloading in osteoarthritis *Adv. Healthcare Mater.* **14** 2501588

[47] Mainardi A, Occhetta P and Rasponi M 2022 Mechanical induction of osteoarthritis traits in a cartilage-on-a-chip model *Methods Mol. Biol.* **2373** 231–51
[48] Bartels E M, Fairbank J C T, Winlove C P and Urban J P G 1998 Oxygen and lactate concentrations measured *in vivo* in the intervertebral discs of patients with scoliosis and back pain *Spine* **23** 1–8
[49] Risbud M V, Schipani E and Shapiro I M 2010 Hypoxic regulation of nucleus pulposus cell survival: from niche to notch *Am. J. Pathol.* **176** 1577
[50] Lv F, Leung V Y L, Huang S, Huang Y, Sun Y and Cheung K M C 2014 In search of nucleus pulposus-specific molecular markers *Rheumatology* **53** 600–10
[51] Rodrigues-Pinto R, Richardson S M and Hoyland J A 2013 Identification of novel nucleus pulposus markers: interspecies variations and implications for cell-based therapies for intervertebral disc degeneration *Bone Joint Res.* **2** 169–78
[52] Rutgesy J, Creemersy L B, Dherty W, Milzz S, Sakaix D, Mochidax J, Aliniz M and Gradz S 2010 Variations in gene and protein expression in human nucleus pulposus in comparison with annulus fibrosus and cartilage cells: potential associations with aging and degeneration *Osteoarthr. Cartil.* **18** 416–23
[53] Minogue B M, Richardson S M, Zeef L A H, Freemont A J and Hoyland J A 2010 Characterization of the human nucleus pulposus cell phenotype and evaluation of novel marker gene expression to define adult stem cell differentiation *Arthritis Care Res.* **62** 3695–705
[54] Dönges L, Damle A, Mainardi A, Bock T, Schönenberger M, Martin I and Barbero A 2024 Engineered human osteoarthritic cartilage organoids *Biomaterials* **308** 122549
[55] Chan S C W, Walser J, Käppeli P, Shamsollahi M J, Ferguson S J and Gantenbein-Ritter B 2013 Region specific response of intervertebral disc cells to complex dynamic loading: an organ culture study using a dynamic torsion-compression bioreactor *PLoS One* **8** 72489
[56] Stokes I A F and Iatridis J C 2004 Mechanical conditions that accelerate intervertebral disc degeneration: overload versus immobilization *Spine* **29** 2724–32
[57] Tavana S, Masouros S D, Baxan N, Freedman B A, Hansen U N and Newell N 2021 The effect of degeneration on internal strains and the mechanism of failure in human intervertebral discs analyzed using digital volume correlation (DVC) and ultra-high field MRI *Front. Bioeng. Biotechnol.* **8** 610907
[58] Ohta R, Tanaka N, Nakanishi K, Kamei N, Nakamae T, Izumi B, Fujioka Y and Ochi M 2012 Heme oxygenase-1 modulates degeneration of the intervertebral disc after puncture in Bach 1 deficient mice *Eur. Spine J.* **21** 1748–57
[59] Leijten J C H, Bos S D, Landman E B M, Georgi N, Jahr H, Meulenbelt I, Post J N, van Blitterswijk C A and Karperien M 2013 GREM1, FRZB and DKK1 mRNA levels correlate with osteoarthritis and are regulated by osteoarthritis-associated factors *Arthritis Res. Ther.* **15** R126
[60] De Luca P *et al* 2020 Intervertebral disc and endplate cell characterisation highlights annulus fibrosus cells as the most promising for tissue-specific disc degeneration therapy *Eur. Cell. Mater.* **39** 156–70
[61] Lopez M A, Pardo P S, Mohamed J S and Boriek A M 2024 ANKRD1 expression is aberrantly upregulated in the mdm mouse model of muscular dystrophy and induced by stretch through NFκB *J. Muscle Res. Cell Motil.* **45** 191–200
[62] Mohamed J S and Boriek A M 2012 Loss of desmin triggers mechanosensitivity and up-regulation of Ankrd1 expression through Akt-NF-κB signaling pathway in smooth muscle cells *FASEB J.* **26** 757–65
[63] Kaneko K, Ito M, Naoe Y, Lacy-Hulbert A and Ikeda K 2014 Integrin αv in the mechanical response of osteoblast lineage cells *Biochem. Biophys. Res. Commun.* **447** 352–7
[64] Embry Flory J J, Fosang A J and Knudson W 2006 The accumulation of intracellular ITEGE and DIPEN neoepitopes in bovine articular chondrocytes is mediated by CD44 internalization of hyaluronan *Arthritis Rheum.* **54** 443–54
[65] Randau T M, Schildberg F A, Alini M, Wimmer M D, Haddouti E-M, Gravius S, Ito K, Stoddart M J and Matsumoto T 2013 The effect of dexamethasone and triiodothyronine on terminal differentiation of primary bovine chondrocytes and chondrogenically differentiated mesenchymal stem cells *PLoS One* **8** e72973
[66] Liang C Z, Li H, Tao Y Q, Zhou X P, Yang Z R, Xiao Y X, Li F C, Han B and Chen Q X 2012 Dual delivery for stem cell differentiation using dexamethasone and bFGF in/on polymeric microspheres as a cell carrier for nucleus pulposus regeneration *J. Mater. Sci. Mater. Med.* **23** 1097–107
[67] Grodzinsky A J, Wang Y, Kakar S, Vrahas M S and Evans C H 2017 Intra-articular dexamethasone to inhibit the development of post-traumatic osteoarthritis *J. Orthop. Res.* **35** 406–11
[68] Sorrentino G *et al* 2017 Glucocorticoid receptor signalling activates YAP in breast cancer *Nat. Commun.* **8** 1–14
[69] Chen S-H, Masuno K, Cooper S B and Yamamoto K R 2013 Incoherent feed-forward regulatory logic underpinning glucocorticoid receptor action *Proc. Natl Acad. Sci. USA* **110** 1964–9
[70] Ciapetti G, Granchi D, Devescovi V, Leonardi E, Greggi T, Di Silvestre M and Baldini N 2012 Ex vivo observation of human intervertebral disc tissue and cells isolated from degenerated intervertebral discs *Eur. Spine J.* **21** 10–19
[71] Wu Z-L, Xie Q-Q, Liu T-C, Yang X, Zhang G-Z and Zhang H-H 2021 Role of the Wnt pathway in the formation, development, and degeneration of intervertebral discs *Pathol. Res. Pract.* **220** 153366
[72] Gorth D J, Lothstein K E, Chiaro J A, Farrell M J, Dodge G R, Elliott D M, Malhotra N R, Mauck R L and Smith L J 2015 Hypoxic regulation of functional extracellular matrix elaboration by nucleus pulposus cells in long-term agarose culture *J. Orthop. Res.* **33** 747–54
[73] Risbud M V, Schoepflin Z R, Mwale F, Kandel R A, Grad S, Iatridis J C, Sakai D and Hoyland J A 2015 Defining the phenotype of young healthy nucleus pulposus cells: recommendations of the spine research interest group at the 2014 annual ORS meeting *J. Orthop. Res.* **33** 283–93
[74] McDonnell E E and Buckley C T 2022 Two- and three-dimensional *in vitro* nucleus pulposus cultures: an in silico analysis of local nutrient microenvironments *JOR Spine* **5** e1222
[75] Jia S *et al* 2024 Single-cell sequencing reveals cellular heterogeneity of nucleus pulposus in intervertebral disc degeneration *Sci. Rep.* **14** 1–15
[76] Sowa G A, Coelho J P, Bell K M, Zorn A S, Vo N V, Smolinski P, Niyonkuru C, Hartman R, Studer R K and Kang J D 2011 Alterations in gene expression in response to compression of nucleus pulposus cells *Spine J.* **11** 36–43
[77] Iatridis J C, MacLean J J, Roughley P J and Alini M 2006 Effects of mechanical loading on intervertebral disc metabolism *in vivo J. Bone Jt. Surg.* **88** 41–46
[78] Takeoka Y, Kanda Y, Kang J D and Mizuno S 2023 Regenerative capability of human nucleus pulposus cells in degenerated disc under hydrostatic pressure mimicking physiologically relevant intradiscal pressure *in vitro Spine* **48** 728–36
[79] Hiyama A, Yokoyama K, Nukaga T, Sakai D and Mochida J 2013 A complex interaction between Wnt signaling and TNF-α in nucleus pulposus cells *Arthritis Res. Ther.* **15** 1–11
[80] Quan M, Park S-E, Lin Z, Hong M-W, Park S-Y and Kim Y-Y 2015 Steroid treatment can inhibit nuclear localization of members of the NF-κB pathway in human disc cells stimulated with TNF-α *Eur. J. Orthop. Surg. Traumatol.* **25** 43–51
[81] Bougault C, Aubert-Foucher E, Paumier A, Perrier-Groult E, Huot L, Hot D, Duterque-Coquillaud M, Mallein-Gerin F and Beier F 2012 Dynamic compression of chondrocyte-agarose constructs reveals new candidate mechanosensitive genes *PLoS One* **7** e36964

[82] Liang C et al 2020 Moderate fluid shear stress regulates heme oxygenase-1 expression to promote autophagy and ECM homeostasis in the nucleus pulposus cells *Front. Cell Dev. Biol.* **8** 127
[83] Nims R J et al 2021 A synthetic mechanogenetic gene circuit for autonomous drug delivery in engineered tissues *Sci. Adv.* **7** 9858–85
[84] Mark Kim M K, Lawrence M, Quinonez D, Brooks C, Ramachandran R and Séguin C A 2024 Transient receptor potential vanilloid 4 regulates extracellular matrix composition and mediates load-induced intervertebral disc degeneration in a mouse model *Osteoarthr. Cartil.* **32** 881–94
[85] Krupkova O, Zvick J and Wuertz-Kozak K 2017 The role of transient receptor potential channels in joint diseases *Eur. Cells Mater.* **34** 180–201
[86] Regehr K J, Domenech M, Koepsel J T, Carver K C, Ellison-Zelski S J, Murphy W L, Schuler L A, Alarid E T and Beebe D J 2009 Biological implications of polydimethylsiloxane-based microfluidic cell culture *Lab Chip* **9** 2132–9
[87] Herland A et al 2020 Quantitative prediction of human pharmacokinetic responses to drugs via fluidically coupled vascularized organ chips *Nat. Biomed. Eng.* **4** 421–36
[88] Gantenbein B, Grünhagen T, Lee C R, Van Donkelaar C C, Alini M and Ito K 2006 An *in vitro* organ culturing system for intervertebral disc explants with vertebral endplates: a feasibility study with ovine caudal discs *Spine* **31** 2665–73
[89] Crump K B, Kanelis E, Segarra-Queralt M, Pascuet-Fontanet A, Bermudez-Lekerika P, Alminnawi A, Geris L, Alexopoulos L G, Noailly J and Gantenbein B 2025 TNF induces catabolism in human cartilaginous endplate cells in 3D agarose culture under dynamic compression *Sci. Rep.* **15** 1–16
[90] Son H-G, Hwang M-H, Lee S, Kim A-G, Kim T-W, Kim J-H, Choi H and Jeong S 2023 Intervertebral disc organ-on-a-chip: an innovative model to study monocyte extravasation during nucleus pulposus degeneration *Lab Chip* **23** 2819–28
[91] Ehrbar M, Rizzi S C, Schoenmakers R G, San Miguel B, Hubbell J A, Weber F E and Lutolf M P 2007 Biomolecular hydrogels formed and degraded via site-specific enzymatic reactions *Biomacromolecules* **8** 3000–7
[92] Urrutia J, Besa P, Campos M, Cikutovic P, Cabezon M, Molina M and Cruz J P 2016 The Pfirrmann classification of lumbar intervertebral disc degeneration: an independent inter-and intra-observer agreement assessment *Eur. Spine J.* **25** 2728–33
[93] Kasamkattil J et al 2023 Human 3D nucleus pulposus microtissue model to evaluate the potential of pre-conditioned nasal chondrocytes for the repair of degenerated intervertebral disc *Front. Bioeng. Biotechnol.* **11** 1119009
[94] Cho J-H, Lee S-K, Lee J-W and Kim E-C 2010 The role of heme oxygenase-1 in mechanical stress- and lipopolysaccharide-induced osteogenic differentiation in human periodontal ligament cells *Angle Orthod.* **80** 740
[95] Panciera T, Azzolin L, Cordenonsi M and Piccolo S 2017 Mechanobiology of YAP and TAZ in physiology and disease *Nat. Rev. Mol. Cell Biol.* **18** 758–70
[96] Wette S G, Birch N P, Soop M, Zügel M, Murphy R M, Lamb G D and Smith H K 2021 Expression of titin-linked putative mechanosensing proteins in skeletal muscle after power resistance exercise in resistance-trained men *J. Appl. Physiol.* **130** 545–61
[97] Bankhead P et al 2017 QuPath: open source software for digital pathology image analysis *Sci. Rep.* **7** 1–7